Bitlis Eren University Journal of Science and Technology

Bitlis Eren Üniversitesi Bilim ve Teknoloji Dergisi

Contact:

Bitlis Eren University Journal of Science and Technology

Bitlis Eren University Journal of Science and Technology

Yıl/Year: 2020 • Cilt/Volume: 10 • Sayı/Issue: 1

Bitlis Eren University Journal of Science and Technology

Yıl/Year: 2020 • Cilt/Volume: 10 • Sayı/Issue: 1

Bitlis Eren University Journal of Science and Technology

Articles

Hakemler / Reviewers

Reviewer	Institution	Number of reviewed articles
Dr. Lecturer Hayriye Esra AKYÜZ	Bitlis Eren University	1
Assoc. Prof. Dr. Hüseyin NARCI	Mersin University	1
Prof. Dr. İsmail Hakkı SARPÜN	Akdeniz University	2
Assoc. Prof. Dr. Mustafa Hicabi BÖLÜKDEMİR	Gazi University	1
Prof. Dr. Eyyup TEL	Osmaniye Korkut Ata University	1
Assoc. Prof. Dr. Sultan Şahin BAL	Bitlis Eren University	1
Assoc. Prof. Dr. Ayşegül KAHRAMAN	Uludağ University	1
Dr. Lecturer Şadiye ÇAKMAK	Eskişehir Osmangazi University	1
Prof. Dr. Atalay KÜÇÜKBURSA	Kütahya Dumlupınar University	1
Dr. Lecturer Mehmet Emin ÖNCÜ	Dicle University	1
Res. Asst. İbrahim Baran KARAŞİN	Dicle University	1
Dr. Lecturer Erdal ÖĞÜN	Van Yüzüncü Yıl University	1
Assoc. Prof. Dr. Fatiğ ÇIĞ	Siirt University	1
Dr. Lecturer Seda OĞUR	Bitlis Eren University	1
Assoc. Prof. Dr. Fatih Çağlar ÇELİKEZEN	Bitlis Eren University	1

Evaluation of motorcycle accidents admitted to the emergency service and the relationship of alcohol with other demographic properties in motorcycle accidents

Ayşen Dikici Ersan[a],* (iD), Zeynep Karakaya[b] (iD), Fatih Esat Topal[b] (iD), Umut Payza[b] (iD), Pınar Yeşim Akyol[b] (iD)

[a]Department of Emergency Medicine, Akhisar Mustafa Kirazoğlu State Hospital, Manisa, Turkey,

[b]Department of Emergency Medicine, Katip Çelebi University, Atatürk Training and Research Hospital İzmir, Turkey

ARTICLE INFO

ABSTRACT

Objective: Motorcycle accidents progress with higher mortality than other accidents. There can be many different factors in the emergence of accidents. The aim of this study is to evaluate the effects of alcohol and other demographic characteristics on motorcycle accidents. Materials and Methods: Patients who were admitted to the emergency department after motorcycle accidents between 01.10.2013-01.10.2014 were evaluated retrospectively. Features such as blood ethanol levels, age, sex, time of admission to the emergency department (hour, day, month and season), weather conditions, mortality, hospitalization and operation necessity and the loss of labor were discussed. Findings: 241 patients were included in the study where 99.2% of the patients were male and the mean age was $27,04 \pm 10,86$. Most of the accidents are found to have occurred in the evening (49.8%), in autumn (31%) and sunny/outdoor conditions (51%) with good visibility. It was determined that 3 patients died due to head trauma, 142 patients were evaluated and discharged from the emergency department and 41 patients were determined to have labor loss longer than 1 month. Conclusion: In motorcycle accidents, mostly young males have been affected. Most of the alcoholic patients (50%) consist of young patients aged between 18-40 years. It has been revealed that head trauma is an important cause of mortality and morbidity in such accidents.

1. Introduction

In developing countries where highways are used more frequently, traffic accidents remain a major problem. Despite the advances in vehicle and road technology, improved safety equipment, and increased training and warning activities, loss of life, disability, loss of labor and economic losses continue to increase. Not only more than one million people die every year in traffic accidents, but also 20 to 50 million injuries occur. 90% of these accidents occur in developing countries. Although trauma management has improved in developed countries, motor vehicle accidents, especially under 44, are still the leading cause of death in the world (1). There may be an increase in traumatic injuries (traffic accidents, falls, violence incidents) due to psychological and mental health problems associated with alcohol use. These traumas, which may be related to alcohol use, constitute 23% of emergency department admissions (2,3). The use of alcohol in drivers is regulated by rules in many countries due to the fact that the traffic accident is one of the most dangerous consequences of alcohol use. While some of the drivers prefer motorcycles for economic reasons and its ease of use, as well as traffic density and parking problems in big cities, some others prefer motorcycles to facilitate and accelerate the works and save

* Corresponding author.
Ayşen DİKİCİ ERSAN
e-mail: aysendikici@gmail.com

time. With the increase in the use of motorcycles, we also encounter accidents more often. In this study, demographic characteristics of patients admitted to the emergency department after motorcycle accidents were discussed.

2. Materials and methods

2.1 The study plan

This study is a retrospective descriptive study. Permission for the study was obtained from İzmir Katip Çelebi University Atatürk Training and Research Hospital Ethics Committee. The study was planned in Izmir Katip Çelebi University Atatürk Training and Research Hospital Emergency Department between 01.10.2013 and 01.10.2014.

Those who ride on motorcycles, accidents involving motorcycle collisions with another motor or non-motorized vehicle are included in the study whereas pedestrians who were injured by a motorcycle or bicycle were not included in the study. The patients, who were not known to have motorcycle injuries, who were not traumatized, who lacked information in their files and who left the hospital voluntarily without any physical examinations were not included in the study. The data on the ages, genders, time of admission to the Emergency Department (hour, day, month) were classified. The blood ethanol levels, whether or not consultations were made, diagnoses in hospitalization, discharge and death and the data on the mechanisms of accidents related data were evaluated.

Parameters took places such as the presence of personal protective measures and driver's license, abnormal physical examination findings, Glasgow Coma Scale (GCS) score, radiological findings, final diagnoses, consultation rates, hospitalization periods and hospital stay. Data obtained were computerized from the forms.

2.2 Statistical Analyses

Data were recorded in Microsoft Office 2007 Excel and SPSS (Statistical Package of Social Sciences) 20 for Windows statistical programs.

Descriptive statistical methods (percentage, mean and standard deviation) were used to evaluate the study data. $p < 0.05$ was considered statistically significant. $P < 0.05$ was considered statistically significant.

3. Findings

241 patients who met the criteria were included in our study (Table 1). While 239 (99.2%) of the cases were male and 2 (0.8%) were female, and the mean age was 27.04 ± 10.865. 170 patients (70.5%) were in the 18-40 age range.

Table 1. General characteristics of patients

		n	%
Age	<18	34	14.1
	18-40	171	71.0
	>40	36	14.9
Gender	Female	2	.8
	Male	239	99.2
Admission Time	08:00-16:00	84	34.9
	16:01-00:00	120	49.8
	00:01-07-59	37	15.4
Day	Monday	33	13.7
	Tuesday	33	13.7
	Wednesday	36	14.9
	Thursday	33	13.7
	Friday	42	17.4
	Saturday	30	12.4
	Sunday	34	14.1
Day	Weekdays	177	73.4
	Weekend	64	26.6
Weather Condition	Sunny	123	51.0
	Cloudy	77	32.0
	Rainy	41	17.0
Admission Month	January	14	5.8
	February	17	7.1
	March	21	8.7
	April	20	8.3
	May	22	9.1
	June	19	7.9
	July	15	6.2
	August	27	11.2
	September	30	12.4
	October	16	6.6
	November	29	12.0
	December	11	4.6
Season	Spring	63	26.1
	Summer	61	25.3
	Autumn	75	31.1
	Winter	42	17.4
Ethanol	Less than 50	217	90.0
	50 and more	24	10.0
Consultation	Yes	112	46.5
	No	129	53.5
Hospitalization/ Discharge	Discharged	142	58.9
	Hospitalization	58	24.1
	Leave the clinic without permission / discharged with his own request	40	16.6
	Ex	1	.4
Total Hospitalization + Report Duration	No	139	57.7
	7 days and fewer	28	11.6

8-30 days	33	13.7
More than 30 days	41	17.0

Evaluation of the admission times to the emergency department of patients injured directly showed that 84 (34.9%) of the patients were admitted during working hours (between 08: 00-16: 00), 120 (49.8%) in the evening (16: 01-00: 00), and 37 (15.4%) during the night (00: 01-07: 59). Most of the accidents were found to have happened in September (12.4%) and in November (12%) and the fewest were in December (%4.6), while 123 (51%) of the accidents occurred in normal weather/road conditions, 77 (32%) occurred in cloudy/overcast weather conditions and 41 (17%) occurred in rainy weather conditions.

Evaluations of the injuries of the patients showed 155 patients (64.3%) had isolated limb injuries, 33 patients (13.7%) had a head injury, 32 patients (13.3%) had facial injuries and 3 patients (1.2%) did not have any injuries. Multiple body traumas were found in 79 patients (32.8%) (Table 2).

Table 2. Distribution of traumas of patients according to body regions

Zone of Injury	(n)	%
1-No Injury	3	1.2
2-Head	33	13.7
3-Face	32	13.3
4-Spinal	16	6.6
5-Thorax	8	3.3
6-Abdomen	11	4.6
7-Pelvis	6	2.5
8-Extremity	155	64.3

It was determined that 142 patients (58.9%) were discharged from the emergency department, 40% (16.6%) of the patients left the emergency room without permission or refused treatment, 58 patients (24.1%) were admitted to the relevant departments, 1 patient (0.4%) died in the emergency department and 2 patients died due to cranial trauma in the intensive care unit

It was found that 139 (57.7%) patients were able to return to their working life the following day after examinations and treatments performed in the emergency department, and 28 (11.6%) were able to work in less than 1 week,33 (%13,7) had a medical report to rest and recuperate for 1 week to 30 days, and that 41 (17%) had to interrupt their working life for more than 1 month due to health problems.

4. Discussion

The mortality and morbidity of the rider and/or passenger are higher than those of other vehicles in the case of traffic accidents involving vehicles which are more unprotected such as motorcycles and bicycles. Patients who are admitted to the emergency department after motorcycle accidents should be evaluated in terms of death and disability as soon as possible with a multidisciplinary trauma approach.

Being a male is an important factor among the effects which determine the occurrence of the accident according to the WHO (4). In accordance with other studies conducted in our country and abroad, most of the patients we evaluated in our study (99.2%) were male. The male patient ratio was determined as 88.5% by Asırdizer et al. (5) and 94.7% by A. Moskal et al. (6).

The mean age of the patients we evaluated in our study was calculated as 27.04 ± 10.865 (14-61). The majority of the patient age group was in the 18-40 age range, in a total of 170 (70.5%) patients and this situation is consistent with other studies in the literature. In a study conducted in Izmir (7), motorcycle accidents were found to have occurred most frequently in the 24.5-39.4 age group, and in another study by Coben et al. (8), 62% of those injured in motorcycle accidents were reported to have been older than 30 years of age. When we examine the age of motorcycle users according to their blood ethanol levels, the average age of our patients had ethanol levels >50 mg/dl is 35.33. In a similar study conducted by Hang-Tsungliu et al. (9), the mean age of patients with ethanol levels was above 50 mg/dl was found as 39.2 years. The fact that the minimum age for legal motorcycle use is 17 (10), motorcycle use is common among young people, and that the use of motorcycles is not preferred due to health problems in advancing age (such as slow reflexes, balancing problems, and vision problems) may have caused the rise of the most intense patient ages to be between 18-40.

When we evaluated our study according to admission hours, 120 (49.8%) out of 241 admissions to the emergency department were between 16: 01-00: 00 hours and the minimum number of admissions was found to be 37 (15.4%) between 00:01-07:59.In a study conducted by Asirdizer et al. (5), when the admission time of motorcycle and bicycle accidents were examined, it was found that 65.4% of the admissions emerged between 12.01 and 20:00 and these values were close to the data in our study. When we examined our study according to the blood ethanol levels of the patients who were admitted, it was determined that the patients with alcohol admitted intensively between 00: 01 and 7: 59. Liu et al. (9) found that patients with alcohol who admitted to the emergency department after motorcycle accidents had applied to the emergency department generally between 17: 00 and 07: 00. In the same study, it was observed that patients without alcohol were admitted to the hospital during the day (07: 00-17: 00). Admissions mainly between 16: 01-00: 00 may be due to the fact that these hours include when people are not working or the hours they spare the time for themselves, outside of rush hours and peak traffic hours. When we examine the admissions according to the level of

ethanol in the blood, the increase in alcohol consumption after the end of working hours and the closure hours of entertainment venues where alcohol consumption is high, such as cafes and bars are within our time range and maybe the reasons for this time interval shifting to 00: 01-07.

Despite the fact that 41% of injuries related to motorcycle accidents are reported to occur at the weekend (8), in another study (6) 25.6% of motorcycle accidents were found to occur at the weekend. In our study, this rate was found to be 26.55% and most of the injuries related to motorcycle accidents were determined to have occurred on Wednesdays and Fridays, however, no statistical significance was found between the days of the week and the occurrence of accidents (p> 0.05).

While in our study most of the accidents were found to have occurred in autumn months (31.1%), in a similar study conducted by Moskal et al. in France (6), the most frequent accidents were found to have occurred in the summer months (39.4%)and the second most common accidents were found in autumn (%37,5). A significant difference between the number of patients in our study and the number of patients in the study performed by Moskal et al could have caused a difference between the two studies (in our study 241 patients, Moskal et al. 181228 patients).

In a study evaluating fatal motorcycle accidents and vehicle accidents (11), 7.6% of motorcycle riders with alcohol and 10.4% of motorcycle riders without alcohol were found to have had accidents in weather conditions in which the field of vision is bad. In our study, it was found that 8.4% of patients with alcohol and 18% of patients without alcohol had an accident on days when the weather was rainy.

Of the 241 patients included in our study, 24 (10%) of them had blood ethanol levels which are above 50 mg/dl. When the studies examining motorcycle accidents similar to the literature are considered, it was determined in a study conducted by Kasantikul et al. in Thailand (12) that 36.3% of 99.4% patients whose blood ethanol levels could be measured were found to have had alcohol while in the study conducted in the province of Bursa in our country examining traffic accidents (5.5% of accidents included in the study was a motorcycle accident) by Durak et al, 6.9% of the casualties were found to have had alcohol in their system. The difference in the amount of alcohol consumption between regions and the change in the intensity of motorcycle use by regions may have caused a difference between the study conducted in Thailand and other studies conducted in our country.

In our study, 79 patients (32.8%) were found to have multiple body traumas. It was determined that 155 patients (64.3%) had limb injuries. When the literature on the subject is examined, it was seen in the previous studies that motorcycle riders were generally injured in more than one body area (14,15), and the most common injuries were observed in the lower extremity (14,16,17,18). The fact that only helmets and protective goggles are listed on the list of compulsory equipment for motorcycles and that other equipment that is protective of the body are not legally obligated, ensures that people do not show the necessary importance and priority to

these clothes and since the motorcycle is overturned to the right or left at the time of the accident due to the vehicle structure, as a result of this overturning, one side of the driver's body may remain under the motorcycle. Therefore, this could be the reason for extremity injuries in the majority of the accidents.

Cranial injuries are the leading cause of death due to motorcycle accidents as determined in the literature (16,19). In our study, 3 patients died due to head trauma in accordance with the literature. It was stated that one of these patients had died in the emergency department and the other 2 patients had died in the intensive care unit due to cranial trauma.

It was determined that 142 patients (58.9%) included in our study were discharged from the emergency department and 58 patients (24.1%) were admitted to related departments. It was found that 40 patients (69%) were operated on, 7 of whom under emergency conditions, and 18 patients (31%) were hospitalized and had medical treatment. In the study which Durak et al. (13) evaluated the traffic accidents in Bursa province in our country, it was found that 43% of the casualties were discharged from the emergency department, 37% were hospitalized, and 17.4% of patients were referred to another center for further examination and treatment. When the patients whose blood ethanol levels are above 50 mg/dl are examined following their examination and interventions in the emergency department, it was determined that 9 patients (37.5%), were hospitalized for treatment and/or operation and 7 patients (29.2%) were found to be discharged from the emergency department. In our study, no statistically significant difference was found between alcohol use, admission and discharge status (p> 0.05). According to a study by Kasantikul et al. (12), it was found that 45% of patients with alcohol required hospitalization or lost their lives and it was determined that one-fourth of the patients needed hospitalization or lost their lives.

Finally, it was determined that 28 (11.6%) of our patients evaluated in our study were able to return to their normal life following hospitalization and resting for up to 1 week, 33 (13.7%) patients were required to be hospitalized and rested between 1 week and 30 days, 41 (17%) were treated for longer than 1 month and had to have a break in their working life. When the literature related to similar situations is examined, in a study, carried out by Asirdizer et al. (5), examining the cases who were injured in the motorcycle or bicycle accidents, it was found that 32 patients (35.6%) received outpatient treatment, 40 (44.4%) patients were hospitalized for 1 to 10 days and 18 patients (20%) were hospitalized for 10 days. When we examined our study according to the blood ethanol levels of the patients admitted, it was determined that 2 out of 24 patients (8.3%)whose blood ethanol level was found above 50 mg/dl were able to start work after 1 week or less than one-week hospitalization and resting, 3 (12.5%) of them required hospitalization and resting between 1 week and 30 days, 5 patients (20.8%) were treated more for than 1 month and should have a break in their working life and 14 patients were found to have

returned to their normal life after being discharged from the emergency department. Liu et al. (9), in the study in which they examined alcohol-related hospitalization, found that the mean duration of hospitalization of inpatients with alcohol in the hospital and intensive care units was 12 days and 13.2 days in patients without alcohol, and no correlation was found between the day of hospitalization and being with or without alcohol.

5. Limitations

All cases in the study dates could not be included since our study was retrospective and the data in the patient files were insufficient, furthermore, the fact that our study was single-centered and that the emergency department was the 3rd step emergency service in the urban area made our study inadequate in terms of generalization. No information was obtained about the presence of protective equipment of patients or the way the accidents occurred. Demographic characteristics of motorcycle accidents in our country can be better demonstrated in a multi-centered study in which the prospective data can be compiled completely, including rural and urban areas where different levels of emergency services are included.

6. Conclusion

According to the data obtained from our study, it was found that motorcycle accidents due to alcohol occurred mostly in age groups over the age of 40 and during the night (between 00: 00-07: 59), in contrast to the predictions in better weather conditions, and most of the injuries were in the extremities. In addition, no statistically significant difference was determined in demographic data (in terms of the day, month, seasons of admission time, distribution of available trauma areas, hospitalization/discharge status and resting periods after the accident) except the blood ethanol level, distribution of the patients' ages and the hours of admission.

References

1. AmericanCollege of Surgeons Committee on Trauma. Advanced Trauma Life Support for Doctors (ATLS), Student course Manual Tenth Edition, Chicago: The American College of Surgeons, 2018

2. Sayal A, Aydın A, Demirkan K, Işımer A. Alkol kullanımı ve suç oranı Gülhane Tıp Dergisi 2005;47(1) : 14–17.

3. Fabbri A, Marchesini G, Morselli-Labate AM, et al. Positive blood alcohol concentration and road accidents. A prospective study in an Italian emergency department Emerg Med J 2002;19: 210–14

4. Peden M et al.; Eds., 'The World Report on Road Traffic Injury Prevention' Summary. Gneva, World Health Organization Library Cataloguing; 200

5. Aşırdizer M., Yavuz S, Zeyfeoğlu Y ve ark. 2003-2009 Yılları Arasında Celal Bayar Üniversitesi Tıp Fakültesi Adli Tıp Anabilim Dalı Polikliniği'ne Başvurmuş Motosiklet/Motorlu Bisiklet Veya Bisiklet Kazalarında Yaralanmış Olguların Değerlendirilmesi. Adli Tıp Dergisi 2009; 23(3): 17-26

6. Moskal A, Martin JL, Laumon B. Risk factors for injury accidents among moped and motorcycleriders. Accident Analysis and Prevention 49 (2012) 5– 11

7. Topçuoğlu M, Güler H, Koçak A, Aktaş EÖ, Şenol E, Ersel M, Boydak B, Kaya A. Motosiklet ve bisiklet kazaları sebebiyle Ege Üniversitesi Tıp Fakültesi acil servisine başvuran olguların özellikleri. 6. Anadolu Adli Bilimler Kongresi Sözel ve Poster Bildiriler Kitabı (Eds: Aşırdizer M, Yavuz MS) 'nda. Manisa: Celal Bayar Üniversitesi Matbaası. 2007:132-6

8. Coben JH, Steiner CA, Owens P. Motorcycle-related hospitalizations in the United States, 2001. Am J PrevMed. 2004; 27(5): 355-62.

9. Liu HT, Liang CC, Rau CS, Hsu SY andHsieh CH. Alcohol-related hospitalizations of adultmotorcycleriders. World Journal of Emergency Surgery 2015, 10:2 http://www.wjes.org/content/10/1/2

10. Sürücü Belgesi İşlemleri – Sürücü Belgesi Alacaklarda Yaş Şartı. Erişim adresi: http://www.asbis.gov.tr/surucu-belgesi-islemleri.asp

11. Huang WS, Lai CH. Survival risk factors for fatal injured car and motorcycle drivers in single alcohol-related and alcohol-unrelated vehicle crashes. Journal of Safety Research 42 (2011) 93–99

12. Kasantikul V, Ouellet JV, Smith T, Sirathranont J, Panichabhongse V. The role of alcohol in Thailand motorcycle crashes. Accident Analysis and Prevention 37 (2005) 357–366

13. Durak D, Fedakar R, Türkmen N, Akgöz S, Baduroğlu E. Road traffic collisions in Bursa, Turkey, during 2003, 2004 and 2005. Injury, Int. J. Care Injured (2008) 39, 547—553

14. Bachulis, B.L., Sangster,W., Gorrell, G.W., et al., 1988. Patterns of injury in helmeted and nonhelmeted motorcyclists. Am. J. Surg. 155, 708–711.

15. Rogers, C.D., Pagliarello, G., McLellan, B.A., Nelson, W.R., 1991. Mechanism of injury influences thepattern of injuries sustained by patients involved in vehiculartrauma. Can. J. Surg. 34 (3), 283–286.

16. Kraus, J.F., McArther, D.L., Silberman, T.A., 1994a. Epidemiology of mildbrain injury. Semin. Neurol. 14, 1–7.

17. Peek, C., Braver, E.R., Shen, H., et al., 1994. Lower extremity injuries from motorcycle crashes: a commoncause of preventable injury. J. Trauma 37, 358–364.

18. Wladis, A., Boström, L., Nilsson, B., 2002. Injuries in 8927 patients admitted after motor-cyclecrashes in Sweden 1987–1994 inclusive. Eur. J. Surg. 168, 178–192.

19. Ankarath, S., Giannoudis, P.V., Barlow, I., Bellamy, M.C., Matthews, S.J., Smith, R.M., 2002. Injury patterns associated with mortality following motorcycle crashes. Injury 33, 473–477.

Gamow-teller strength and electron capture cross-section calculation by pn-QRPA for selected fp-shell nuclei

Jameel-Un Nabi[a, *] iD, Muhammad Riaz[a] iD, Asim Ullah[a] iD

[a] GIK Institute of Engineering Sciences and Technology, Topi 23640, Khyber Pakhtunkhwa, Pakistan.

ARTICLE INFO

ABSTRACT

The allowed Gamow-Teller (GT) strengths and associated weak interaction rates on fp-shell nuclides are the most familiar processes of spin-isospin ($\sigma\tau$) type. These rates play crucial role in several astrophysical processes, particularly in nuclear synthesis and supernova-explosions. As per simulation consequences, the electron capture cross section on medium-heavy nuclei has a key impact on decreasing the ratio of electron-to-baryon of the stellar matter during the late stages of stars formation. Stellar model based on the theoretical approaches should be tested against the available measured data. In the current work we present calculated Gamow-Teller strength distributions by pn-QRPA model for selected fp-shell nuclei (^{42}Ti, ^{46}Cr, ^{50}Fe and ^{54}Ni) and compare our results with available measured data. The Gamow-Teller strength distributions are well fragmented over the energy range 0-12 MeV and have a good comparison with experimental data. We calculate the electron capture cross-section for selected nuclei at temperature 0.5 MeV, 1.0 MeV and 1.5 MeV that shows the temperature dependence of calculated electron capture cross section for astrophysical applications.

1. Introduction

In study of nucleosynthesis and other astrophysical processes, beta decay plays an important role in analysis of Gamow-Teller (GT) transitions and nuclear half-lives. The GT transitions may be investigated by charge-changing transition reactions under laboratory conditions. But data for GT transitions for most of the unstable nuclei may be provided by many of the theoretical models possessing a decent agreement with experimental data. One such successful nuclear model is the proton-neutron quasi-particle random phase approximation (pn-QRPA) model that provides weak interactions rates under terrestrial as well as stellar conditions [1-4].

Fuller, Fowler, and Newman [5], computed the beta decay weak interactions rates for the first time by using independent particle model (IPM). They tabulated the beta decay rates for many nuclei (21 ≤ A ≤ 60) having importance in astrophysical applications. Later large scale shell model diagonalization model, Shell Model Monte Carlo [6, 7] and pn-QRPA models refined the weak interaction rates for simulation of pre-supernova phenomenon [3, 8, 9]. By improving these weak interaction rates it was concluded that GT strength distributions and electron capture cross-sections (ECC) for fp-shell nuclei play crucial role in providing information for pre-supernova evolution of massive stars.

In this article, we compute GT transitions and ECC for selected fp-shell nuclei by pn-QRPA model. In performing our calculation, we used state by state computation instead of Brink's-Axel hypothesis [10].

* *Corresponding author.*
E-mail address: jameel@giki.edu.pk
ORCID: 0000-0002-8229-8757 (Jameel-un Nabi), 0000-0003-4521-4259 (Muhammed Riaz), 0000-0002-2653-310X (Asım Ullah)

2. Formalism

The pn-QRPA model was used to compute the GT strength distribution and associated ECC on the selected chromium isotopes in the stellar matter. The following Hamiltonian was considered

$$H^{QRPA} = H^{sp} + V_{GT}^{ph} + V_{GT}^{pp} + V^{pair} ,\qquad (1)$$

where H^{sp} is the single particle Hamiltonian, V_{GT}^{ph} and V_{GT}^{pp} are the particle-hole GT force and particle-particle GT force, respectively. The last term V^{pair} represents the pairing force for which the BSC approximation was considered. The single particle energies and wave functions were calculated in Nilsson model [11], in which the nuclear deformation (β_2) was incorporated. The particle-particle and particle-hole parameters were adapted such that the measured energy of the GT giant resonance was reproduced wherever available. The calculated GT strength distributions fulfilled the model independent Ikeda sum rule [12]. The Nilsson-potential parameter (NPP) was taken from Ref. [13] and $\hbar\omega = 41A^{1/3}$ was taken as oscillator constant for both neutrons and protons. Q-values were taken from Ref. [14] and a traditional relation $\Delta_p = \Delta_n = 12/\sqrt{A}$ MeV was considered for pairing gaps.
The electron capture (EC) and positron decay (PD) weak-rates from parent state "m" to daughter state "n" are given by

$$\lambda_{mn}^{EC(PD)} = \ln 2 \frac{f_{mn}^{EC(PD)}(T,\rho,E_f)}{D/B_{mn}} ,\qquad (2)$$

where B_{mn} is the nuclear reduced transition probability and is given by

$$B_{mn} = B(F)_{mn} + (g_A/g_V)^2 B(GT)_{mn} .\qquad (3)$$

The values of D and g_A/g_V were taken as 6143s [15] and -1.254 [16], respectively.
The reduced Fermi ($B(F)_{mn}$) and GT ($B(GT)_{mn}$) transition probabilities are specified by the following

$$B(F)_{mn} = \frac{1}{2J_m+1} \left| \langle n || \sum_k t_+^k || m\rangle \right|^2 ,\qquad (4)$$

$$B(GT)_{mn} = \frac{1}{2J_m+1} \left| \langle n || \sum_k t_+^k \sigma^{\rightarrow k} || m\rangle \right|^2 ,\qquad (5)$$

where J_m is the total spin of the parent state $|m\rangle$, $\sigma^{\rightarrow k}$ is the Pauli spin matrix and t_+^k refer to the iso-spin raising operator. The summation is taken for all the nucleons inside the nucleus. The computation of electron capture cross-section is governed by the weak-interaction Hamiltonian, given by

$$\hat{H}_\omega = \frac{G_F \cos\theta_c}{\sqrt{2}} j_\mu^{lept} \hat{J}^\mu ,\qquad (6)$$

The terms θ_c and G_F in the above equation, stands for Cabibbo angle and Fermi coupling constant, respectively. The $\hat{J}^\mu$ and j_μ^{lept} are the hadronic and leptonic currents, respectively, given by

$$j_\mu^{lept} = \bar{\psi}_{\upsilon_e}(x) \gamma_\mu (1 - \gamma_5) \psi_{\upsilon_e}(x),\qquad (7)$$

$$\hat{J}^\mu = \bar{\psi}_p(x) \gamma_\mu (1 - C_A\gamma_5) \psi_n(x),\qquad (8)$$

where $\psi_{\upsilon_e}(x)$ show the spinor operator. Our main goal was to compute the ECC which is based on nuclear transition matrix elements between initial $|m\rangle$ and final state $|n\rangle$ of parent and daughter nuclei, respectively.

$$\langle n \| \hat{H}_\omega \| m \rangle = \frac{G}{\sqrt{2}} l^\mu \int d^3 x e^{-iq \cdot x} \left\langle n \left| \hat{J}_\mu \right| m \right\rangle \qquad (9)$$

where the q is the three-momentum transfer and $l^\mu e^{-iq \cdot x}$ are the leptonic matrix element which was employed in matrix elements calculation [17, 18]. We used low momentum transfer approximation $q \rightarrow 0$ in this work. By assuming such approximation the transitions of Gamow-Teller (GT) operator ($GT^+ = \sum_i \tau_i^+ \sigma_i$) provide the dominant contribution to the total stellar ECC [19]. The total ECC in the stellar condition as a function of incident energy of projectile electron (E_e) is given by the equation

$$\sigma(E_e, T) = \frac{G_F^2 \cos^2\theta_c}{2\pi} \sum_m F(Z, E_e) \frac{(2J_m+1)\exp\left(\frac{-E_m}{kT}\right)}{G(A,Z,T)}$$

$$\times \sum_{J,f}(E_e - Q + E_m - E_m)^2 \frac{|\langle m|GT^+|n\rangle|^2}{(2J_m+1)} \qquad (10)$$

The terms $F(Z, E_e)$ and $G(A, Z, T)$ are the well-known Fermi and nuclear partition function (NPF), respectively. The last term of Eq. (10) corresponds to the nuclear matrix elements between final and initial states. The calculation of Fermi function was done using the recipe given by Ref. [19]. The NPF was computed using the prescription introduced by Refs. [20, 21].

3. Results and Discussion

The GT strength distributions computed by pn-QRPA for ^{42}Ti, ^{46}Cr, ^{50}Fe and ^{54}Ni are compared with the experimental data and previous calculations [22-28] in Fig. 1. In β-decay experiment the excitation energy up to E_{ex} = 1.888 MeV was considered to probe the GT strength distributions while in charge changing reaction ^{42}Ca(^{3}He, t) a maximum of E_{ex} = 3.688

MeV was considered to measure the GT strength.

In Fig. 1 we also depict shell model (using GXPF1 and KB3G interactions) and pn-QRPA extended GT strength distributions up to E_{ex} = 12 MeV. Calculated GT strength distribution by pn-QRPA have good fragmentation for all energy range up to 12 MeV and are bigger in magnitude than previously calculated and measured results. One notes a decent comparison of the measured and calculated GT strength distributions.
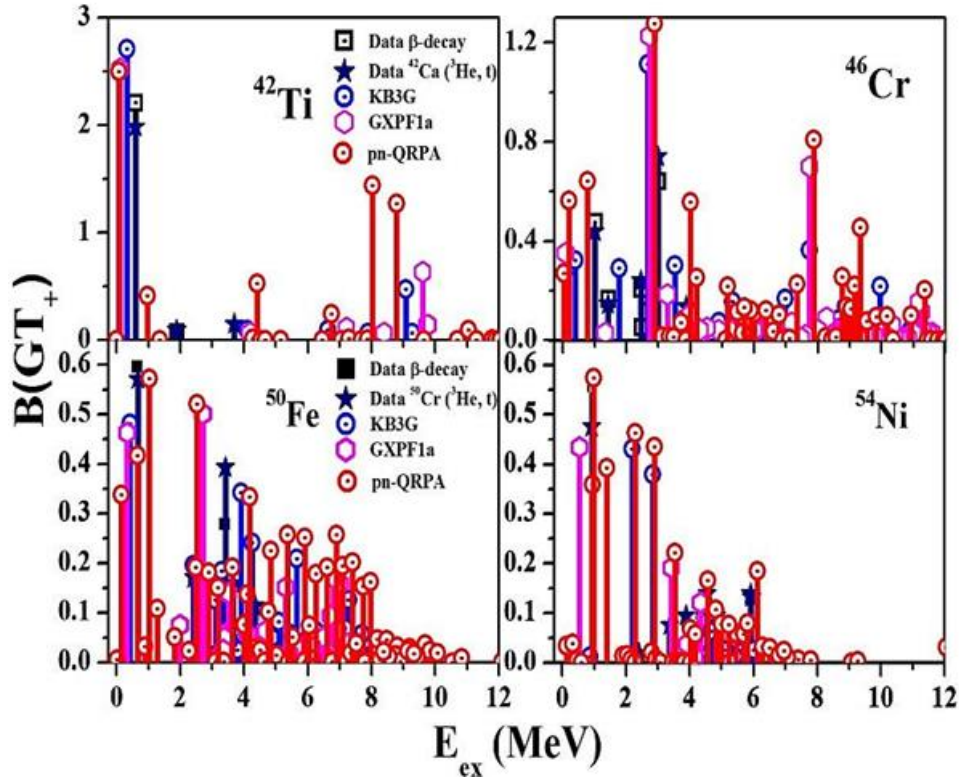
Figure 1. Calculated and measured GT strength distributions for ^{46}Cr, ^{54}Ni, ^{50}Fe and ^{42}Ti as a function of daughter excitation energy. For explanation of legends see text.

Table 1 show the measured and computed GT strength distribution for ^{54}Ni, ^{50}Fe, ^{46}Cr, and ^{42}Ti. The third and fourth column of Table 1 shows the experimental data of β-decay and charge changing reaction, 5th and 6th column represents the shell model data calculated through KB3G and GXPF1

interactions, respectively. Second last and last column display the results of extreme single particle model and pn-QRPA. The difference between measured and calculated data is attributed to the cut-off energies described before. It is noted that the pn-QRPA and extreme single particle model results are bigger than the results of other models.

Table 1. Comparison of measured and computed total GT strengths for selected fp-shell nuclei.

A	N	β-Decay	CER	KB3G	GXPF1a	ESPM	pn-QRPA
54	26	1.082	1.117	12.197	13.362	16.29	18.16
50	24	1.344	1.859	9.464	10.277	14.14	16.97
46	22	2.047	2.219	7.231	7.613	10.70	9.50
42	20	2.372	2.297	6.000	6.000	6.00	7.86

In the last part of our article we describe the results of ECC for selected fp-shell nuclei (^{42}Ti, ^{46}Cr, ^{50}Fe and ^{54}Ni) achieved by employing the pn-QRPA model. These results are shown in Table 2 (^{42}Ti and ^{46}Cr) and Table 3 (^{50}Fe and ^{54}Ni). The calculated ECC is shown as a function of incident electron energy at three different temperature 0.5 MeV, 1.0 MeV and 1.5 MeV. In Table 2 and Table 3 the first column shows the incident electron energy. Further three different temperatures are mentioned for all of nuclei in both the tables.

The comparison of ECC for all selected cases shows almost same trend. As the incident electron energy increases the ECC for the first few MeV increases sharply. This trend in calculated ECC later becomes smooth with further increase in incident electron energy. The calculated ECC have direct impact on GT strength distributions and therefore this trend may be a direct consequence of the calculated GT strength distributions.

To study the effect of ECC on temperature we calculated ECC at three effective temperatures in the range of 0.5 MeV – 1.5 MeV. As the temperature of the core increases from 0.5 MeV to 1.5 MeV the calculated ECC increased on average by two orders of magnitude. This big change is because of thermal unblocking of GT states. As the temperature further increases from 1.0 MeV to 1.5 MeV the calculated ECC increased marginally as the unblocking of states has already taken place. The trend of the calculated ECC is similar for all four cases.

Table 2. Calculated EC cross section (in units of cm^2) for three different temperatures 0.5MeV, 1.0MeV and 1.5MeV for ^{42}Ti and ^{46}Cr.

Energy (MeV)	^{42}Ti			^{46}Cr		
	T=0.5MeV	T=1.0MeV	T=1.5MeV	T=0.5MeV	T=1.0MeV	T=1.5MeV
2	2.25E-48	3.14E-47	3.97E-47	3.39E-48	4.31E-47	5.75E-47
3	5.01E-47	6.97E-46	8.80E-46	7.70E-47	9.79E-46	1.31E-45
4	3.25E-46	4.48E-45	5.66E-45	5.05E-46	6.42E-45	8.57E-45
5	1.22E-45	1.67E-44	2.11E-44	1.91E-45	2.44E-44	3.26E-44
6	3.33E-45	4.54E-44	5.75E-44	5.27E-45	6.74E-44	9.01E-44
7	7.40E-45	1.00E-43	1.28E-43	1.17E-44	1.51E-43	2.03E-43
8	1.42E-44	1.93E-43	2.46E-43	2.24E-44	2.91E-43	3.93E-43
9	2.46E-44	3.37E-43	4.33E-43	3.81E-44	5.04E-43	6.83E-43
10	3.98E-44	5.54E-43	7.22E-43	5.94E-44	8.04E-43	1.10E-42
11	6.21E-44	8.93E-43	1.18E-42	8.65E-44	1.22E-42	1.69E-42
12	9.66E-44	1.45E-42	1.95E-42	1.21E-43	1.79E-42	2.52E-42
13	1.54E-43	2.42E-42	3.30E-42	1.68E-43	2.65E-42	3.80E-42
14	2.53E-43	4.18E-42	5.73E-42	2.40E-43	4.01E-42	5.85E-42
15	4.29E-43	7.35E-42	1.01E-41	3.60E-43	6.33E-42	9.34E-42
16	7.42E-43	1.30E-41	1.79E-41	5.75E-43	1.04E-41	1.54E-41
17	1.29E-42	2.27E-41	3.12E-41	9.65E-43	1.74E-41	2.58E-41
18	2.21E-42	3.90E-41	5.34E-41	1.66E-42	2.94E-41	4.34E-41
19	3.71E-42	6.56E-41	8.94E-41	2.84E-42	4.94E-41	7.24E-41
20	6.12E-42	1.08E-40	1.46E-40	4.82E-42	8.18E-41	1.19E-40
21	9.86E-42	1.72E-40	2.33E-40	8.01E-42	1.33E-40	1.92E-40
22	1.55E-41	2.70E-40	3.63E-40	1.30E-41	2.11E-40	3.03E-40
23	2.39E-41	4.13E-40	5.54E-40	2.06E-41	3.28E-40	4.69E-40
24	3.60E-41	6.19E-40	8.29E-40	3.18E-41	5.00E-40	7.11E-40
25	5.33E-41	9.10E-40	1.22E-39	4.82E-41	7.46E-40	1.06E-39
26	7.74E-41	1.32E-39	1.75E-39	7.15E-41	1.09E-39	1.55E-39
27	1.11E-40	1.87E-39	2.49E-39	1.04E-40	1.58E-39	2.22E-39
28	1.56E-40	2.63E-39	3.49E-39	1.49E-40	2.24E-39	3.14E-39
29	2.16E-40	3.63E-39	4.82E-39	2.10E-40	3.13E-39	4.38E-39
30	2.96E-40	4.96E-39	6.57E-39	2.91E-40	4.31E-39	6.03E-39

* *Corresponding author.*

E-mail address: jameel@giki.edu.pk

ORCID: 0000-0002-8229-8757 (Jameel-un Nabi), 0000-0003-4521-4259 (Muhammed Riaz), 0000-0002-2653-310X (Asım Ullah)

Table 3. Same as Table 2 but for ^{50}Fe and ^{54}Ni.

Energy (MeV)	^{50}Fe			^{54}Ni		
	T=0.5MeV	T=1.0MeV	T=1.5MeV	T=0.5MeV	T=1.0MeV	T=1.5MeV
2	8.34E-48	1.14E-46	1.49E-46	6.80E-48	1.20E-46	1.55E-46
3	1.97E-46	2.68E-45	3.49E-45	1.60E-46	2.81E-45	3.63E-45
4	1.35E-45	1.81E-44	2.36E-44	1.07E-45	1.88E-44	2.43E-44
5	5.33E-45	7.13E-44	9.28E-44	4.17E-45	7.28E-44	9.39E-44
6	1.54E-44	2.05E-43	2.67E-43	1.18E-44	2.06E-43	2.65E-43
7	3.63E-44	4.80E-43	6.25E-43	2.73E-44	4.73E-43	6.09E-43
8	7.39E-44	9.74E-43	1.27E-42	5.42E-44	9.40E-43	1.21E-42
9	1.35E-43	1.78E-42	2.31E-42	9.65E-44	1.68E-42	2.16E-42
10	2.27E-43	2.99E-42	3.90E-42	1.58E-43	2.78E-42	3.57E-42
11	3.57E-43	4.76E-42	6.22E-42	2.44E-43	4.36E-42	5.59E-42
12	5.35E-43	7.26E-42	9.53E-42	3.61E-43	6.60E-42	8.47E-42
13	7.74E-43	1.08E-41	1.43E-41	5.21E-43	9.88E-42	1.27E-41
14	1.10E-42	1.59E-41	2.11E-41	7.49E-43	1.49E-41	1.91E-41
15	1.54E-42	2.35E-41	3.14E-41	1.09E-42	2.27E-41	2.92E-41
16	2.16E-42	3.50E-41	4.71E-41	1.62E-42	3.54E-41	4.56E-41
17	3.07E-42	5.27E-41	7.14E-41	2.48E-42	5.60E-41	7.26E-41
18	4.44E-42	8.03E-41	1.09E-40	3.87E-42	8.97E-41	1.16E-40
19	6.52E-42	1.23E-40	1.69E-40	6.11E-42	1.44E-40	1.87E-40
20	9.70E-42	1.89E-40	2.60E-40	9.69E-42	2.29E-40	2.98E-40
21	1.46E-41	2.90E-40	3.98E-40	1.53E-41	3.61E-40	4.71E-40
22	2.19E-41	4.41E-40	6.05E-40	2.38E-41	5.60E-40	7.31E-40
23	3.27E-41	6.63E-40	9.09E-40	3.67E-41	8.56E-40	1.12E-39
24	4.86E-41	9.84E-40	1.35E-39	5.55E-41	1.29E-39	1.68E-39
25	7.15E-41	1.44E-39	1.98E-39	8.27E-41	1.90E-39	2.48E-39
26	1.04E-40	2.08E-39	2.85E-39	1.21E-40	2.76E-39	3.61E-39
27	1.49E-40	2.97E-39	4.06E-39	1.75E-40	3.96E-39	5.17E-39
28	2.12E-40	4.19E-39	5.72E-39	2.49E-40	5.59E-39	7.30E-39
29	2.97E-40	5.82E-39	7.94E-39	3.49E-40	7.78E-39	1.02E-38
30	4.11E-40	8.00E-39	1.09E-38	4.83E-40	1.07E-38	1.40E-38

4. Conclusion

GT transitions and ECC were calculated for selected fp-shell nuclei by using pn-QRPA model. Our calculated GT strengths results were bigger than previously measured and calculated results. The calculated ECC increases with the incident electron energy as well as with the core temperature. The increase in ECC due to temperature effect is in response of thermal unblocking of GT transitions states. These ECC study maybe of utility in the modeling and simulation of the pre-supernova evolution of massive stars.

References

[1] A. Staudt, E. Bender, K. Muto and H. V. Klapdor Kleingrothaus, At. Data. Nucl. Data. Tables, (1990), 44, 79.

[2] M. Hirsch, A. Staudt, K. Muto and H. V. Klapdor-Kleingrothaus, At. Data and Nucl. Data Tables, (1993), 53, 165-193.

[3] J.-U. Nabi and H. V. Klapdor-Kleingrothaus, Atom. Data and Nucl. Data Tables, (2004), 88, 237.

[4] J.-U. Nabi and H. V. Klapdor-Kleingrothaus, At. Data Nucl. Data Tables, (1999), 71, 149.

[5] G. M. Fuller, W. A. Fowler and M. J. Newman, Astrophys. J. Suppl. Ser, (1980), 42, 447; (1982), 48, 279; Astrophys. J. (1982), 252, 715; (1985), 293, 1.

[6] K. Langanke and G. Martinez-Pinedo, Nucl. Phys. A (2000), 673, 481.

[7] G. Martinez-Pinedo, K. Langanke and D. J. Dean, Astrophys. J. Suppl. Ser, (2000), 126, 493.

[8] A. Heger, K. Langanke, G. Martinez-Pinedo and S. E. Woosley, Phys. Rev. Lett, (2001), 86, 1678.

[9] D. J. Dean, K. Langanke, L. Chatterjee, P. B. Radha and M. R. Strayer, Phys. Rev. C, (1998), 58, 536.

[10] D. Brink, D. Phil. Thesis, Oxford University, Unpublished (1955); P. Axel, Phys. Rev. (1962), 126, 671.

[11] S. G. Nilsson, Mat. Fys. Medd. Dan. Vid. Selsk (1955), 29, 1.

[12] K. Ikeda, S. Fujii and J. I. Fujita, Phys. Lett. (1963), 3 271.

[13] I. Ragnarsson and R. K. Sheline, Phys. Scr. (1984), 29, 385.

[14] P. Moller and J. Randrup, Nucl. Phys. A, (1990), 514, 1.

[15] P. Moller, A. J. Sierk, T. Ichikawa and H. Sagawa, At. Data Nucl. Data Tables (2016), 109, 1.

[16] G. Audi, F. Kondev, M. Wang, W. Huang, and S. Naimi, Chinese physics C, (2017), 41, 030001.

[17] M. Hirsch, A. Staudt, K. Muto and H. V. Klapdor-Kleingrothaus, Nucl. Phys. A, (1991), 535, 62.

[18] K. Muto, E. Bender and H. V. Klapdor, Z. Phys. A Atom. Nuc. A, (1989), 333, 125.

[19] K. Nakamura, (Particle Data Group): J. Phys. G, Nucl. Part. Phys. (2010), 37, 075021.

[20] N. B. Gove and M. J. Martin, At. Data Nucl. Data Tables (1971), 10, 205.

[21] C. D. Goodman, C. A. Goulding, M. B. Greenfield, J. Rapaport, D. E. Bainum, C. C. Foster, W. G. Love and F. Petrovich, Phys. Rev. Lett., (1980), 44, 1755.

[22] F. Molina, B. Rubio, Y. Fujita, W. Gelletly, J. Agramunt, A. Algora, J. Benlliure, P. Boutachkov, L. Cceres, R. B. Cakirli and E. Casarejos, Physical Rev. C, (2015), 91, 014301.

[23] T. Adachi, Y. Fujita, P. Von Brentano, A. F. Lisetskiy, G. P. A. Berg, C. Fransen, D. De Frenne, H. Fujita, K. Fujita, K. Hatanaka and M. Honma, Physical Rev. C, (2006), 73 024311.

[24] Y. Fujita, T. Adachi, P. Von Brentano, G. P. A. Berg, C. Fransen, D. De Frenne, H. Fujita, K. Fujita, K. Hatanaka, E. Jacobs and K. Nakanishi, Physical Rev. let, (2005), 95, 212501.

[25] T. Adachi, Y. Fujita, P. Von Brentano, G. P. A. Berg, C. Fransen, D. De Frenne, H. Fujita, K. Fujita, K. Hatanaka, M. Honma and E. Jacobs, Nucl. Phys. A, (2007), 788, 70-75.

[26] T. Adachi, Y. Fujita, A. D. Bacher, G. P. A. Berg, T. Black, D. De Frenne, C. C. Foster, H. Fujita, K. Fujita, K. Hatanaka and M. Honma, Phys. Rev. C, (2012), 85, 024308.

[27] V. Kumar and P. C. Srivastava, The Eur. Phys. J. A 52 (2016) 181.

Internal bremsstrahlung spectrum of $^{86}_{37}$Rb for forbidden beta transition

Ekrem Almaz [a,*] ⓘD , Emrullah Tokgöz [b] ⓘD

[a] Muş Alparslan University, Science & Literature Faculty, Physics Department, Güzeltepe Campus, 49250, Muş, Turkey
[b] Muş Alparslan University, İnstitute of Science, Güzeltepe Campus, 49250, Muş, Turkey

ARTICLE INFO

ABSTRACT

Many researchers have worked on to explain the theory of internal bremsstrahlung process released along with a beta particle and a neutrino from the beta-decaying radioactive nuclei. According to the original Knipp, Uhlenbeck and Bloch (KUB) theory, IB is a low-intensity continuous spectrum of electromagnetic radiation which accompanies all types of beta decay. Former experimental studies on the internal bremsstrahlung emission from the forbidden beta transitions have shown marked deviations from the theoretical calculations. We took the more theoretical calculations for the IB probability problem. The analytical expressions proposed by the work of Chang and Falkoff for forbidden transitions were used for the IB spectrum. We have also calculated the Coulomb effects of IB spectrum from the study by Lewis and Ford who first addressed to these phenomena. We have handled and analyzed the data of IB emissions of $^{86}_{37}$Rb beta emitting isotope that its transition is classified as forbidden. In addition to the analytical calculation, IB spectrum was also obtained by applying Monte Carlo Method to IB problem. The results were compared with the IB spectrum results which are calculated from the analytical expressions.

1. Introduction

The disintegration of the nucleus by emitting electrons or positron, or the capture of one of the electrons around the nucleus orbits, is called beta decay. There is no change in the mass number of the nucleus, but there is always a change in the nuclear charge after the disintegration. During this disintegration, a beta particle (electron or positron) and a neutrino with daughter nucleus is released into the medium. Beta particles emitted from radioactive nuclei have a continuous energy distribution. Beta particles have kinetic energy from zero to a maximum value with various possibilities. The energy of disintegration is shared among the beta, the recoil nuclei and neutrino/antineutrino. Therefore, in beta decay, it has been shown that the sharing of disintegration energy between the beta particle and neutrino or antineutrino is random [1]. Thus, the beta particles have a continuous energy spectrum from E = 0 to a maximum energy value E = E_m. The quantum mechanical theory of beta spectrum was developed by Fermi [2, 3]. The total energy of a beta particle having an energy E in the unit of electron rest mass energy is;

$$W = \frac{E}{mc^2} + 1 \qquad (1)$$

The number of beta particles in the energy range W and W+dW, is given by [4, 1, 2, 3];

$$N(W)dW = \frac{|P|^2}{\tau_0} F(Z,W)(W^2-1)^{1/2}(W_0-W)^2 W dW \quad (2)$$

Here $|P|^2$ is the square of the matrix element for the transition. τ_0 is the time constant and F(Z, W) is a complex function defined as the electron density ratio. This study was performed for β^- particles and β^+ particles were not considered.

The speed of the electron In terms of the speed of light, depending on W can be written as

$$\beta = (W^2-1)^{1/2} \qquad (3)$$

* Corresponding author.
  Tel.: +90436 2494949-1555; fax: +90 436 2491022
  E-mail address: e.almaz@alparslan.edu.tr,
  ORCID: 0000-0002-8708-2189 (Ekrem.almaz), 0000-0002-6486-2019 (Emrullah.tokgöz)

The following expression is obtained for electrons, i.e. beta particles, if the Eq.(3) of beta is written as in the equation given by Almaz [5],

$$F(Z, W) \approx 2\pi \alpha Z \, W / (W^2 - 1)^{1/2} \qquad (4)$$

If this expression is used in Eq.(2), the energy spectrum of beta particles can be expressed as,

$$N(W) = \frac{|P|^2}{\tau_0} 2\pi \alpha Z (W_0 - W)^2 W^2 \qquad (5)$$

There are some differences in the basic properties of beta disintegration. The smaller the square of the transition matrix $|P|^2$ seen in the Eq.(5) (the greater the f t), the more impossible the transition is considered, i.e. prohibited. Such transitions are called forbidden transitions. The greater the $|P|^2$ (the smaller the f t), the more the transition is possible which means allowed. Such transitions are called allowed transitions. The value of $|P|^2$ is proportional to the amount of superposition of the wave functions of the mother nucleus and daughter nucleus. The more the wave functions overlap, the greater the value $|P|^2$ and approach the value 1. The f t values for the various beta transitions range from 10^3 (super-allowed transitions) to 10^{23} (most forbidden transitions).

The magnitude of P depends on the selection rules as in the gamma decay and the magnitude of the L_β orbital angular momentum which is taken away by the $\beta^-, \bar{v} \ / \beta^+, v$ beta pair from the daughter nucleus. When L_β increases by one degree, $|P|^2$ becomes smaller by $10^{-2} - 10^{-4}$, therefore, the probability of transition is reduced. For the most allowed transitions, the angular momentum carried by the pair $\beta^-, \bar{v} \ / \beta^+, v$ is zero. Therefore the transitions are allowed for $L_\beta = 0$. Transitions for $L_\beta = 1$ are first forbidden and for $L_\beta = 2$ are second forbidden.

The theoretical energy spectrum obtained from Eq. (5) for Rb-86 β^- source with Z value of 37 is given in Figure 1.
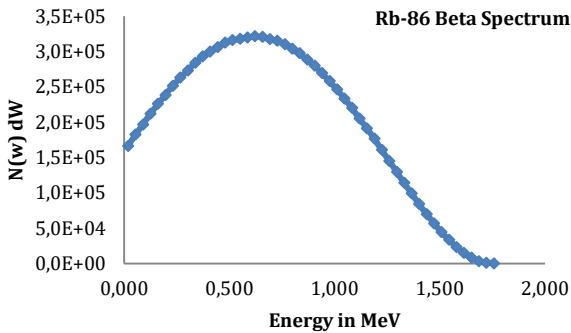

Figure 1. Energy spectrum of beta distribution of Rb-86 isotope

2. Internal Bremsstrahlung (IB) Spectrum from Rb-86 Isotope

There is a certain likelihood of a photon emission simultaneously along with the beta particle and neutrino/anti-neutrino in beta decay mechanism. IB photons have a distinguishing distribution and they are in the form of a continuous photon spectrum as well. The IB photon is caused by the sudden change of electric charge in the nucleus at the moment of release of the beta particle emitted from the radioactive source. for the reason of that this nuclear event is called the Internal Bremsstrahlung (IB) for the sake of distinguishing it from the External Bremsstrahlung (EB) caused by the loss of radiative energy with other particles rather than the nucleus from which the electron emerges. Knipp, Uhlenbeck [6] and independently Bloch [7] presented the IB theory for allowed beta transitions, without taking into account Coulomb effects. Wang Chang and Falkoff [8] have extended The KUB theory for the first and second forbidden transitions. Nilsson [9], Lewis and Ford [10] and Spruch and Gold [11] have calculated the IB spectra considering the Coulomb effects of the nucleus. For beta decays of forbidden transitions, IB spectra were first discussed by Lewis and Ford [10]. The solutions of the first proposed KUB theory were found to be incompatible with experimental data at the midpoint and high energy region of the spectrum. Further theoretical calculations were made by Ford and Martin [12] for the possibility of IB that the detour transitions, a distinctive behavior accompanying the forbidden transitions of the nucleus, were taken into consideration in their studies. As a result, some improvements have been achieved in the agreement between the theory developed by Ford and Martin [12] and the experiments.

In this study, the analytical solutions proposed by Chang and Falkoff [8] for the purpose of having the IB photon spectra for first forbidden beta transitions were calculated as well as Monte Carlo Method for IB problem in computer environment. Thus the IB spectrum of Rb-86 has calculated via this way.

2.1. IB Spectrum by Monte Carlo Simulation Technique

The β^- particle energy is sampled between a cutoff energy value of $E_c = 10$ keV and the endpoint energy of E_m. For the sampling process, it is not possible to find an analytical expression by applying the basic Monte Carlo principle to the energy distribution of β^- particles given by Eq. (5). Therefore, the Rejection Method is used for sampling the distribution [13, 15]. In the execution of the Rejection Method, the rectangular rejection function was used. Detailed calculations related to Monte Carlo method were applied as given in Almaz and Almaz and Cengiz [5, 13]. The IB spectrum obtained by the Monte Carlo Method for Rb-86 was compared with the IB spectrum of the same isotope obtained for forbidden transitions.

2.2. IB spectrum for Allowed and Forbidden Transitions

The distribution theory of the IB spectrum for allowed transitions is in the notation of Chang and Falkoff [10] if $x = W_0$-k:

$$S(k) = \frac{\alpha G^2}{8\pi^4} \frac{2}{15} |R_{\alpha\beta}|^2 \frac{1}{k} \left\{ \left[\frac{58}{63} x^9 - \frac{86}{21} W_0 x^8 + \frac{488}{63} W_0^2 x^7 - \frac{364}{45} W_0^3 x^6 + \frac{151}{30} W_0^4 x^5 - \frac{11}{6} W_0^5 x^4 + \frac{1}{3} W_0^6 x^3 \right] ln2x - \left[\frac{151553}{79380} x^9 - \frac{72661}{8820} W_0 x^8 + \frac{33142}{2205} W_0^2 x^7 - \frac{1138}{75} W_0^3 x^6 + \frac{16577}{1800} W_0^4 x^5 - \frac{239}{72} W_0^5 x^4 + \frac{11}{18} W_0^6 x^3 \right] \right\} \qquad (6)$$

IB spectrum in scalar interaction for isotopes with first forbidden beta transitions is given by,

$$S(k) = \frac{\alpha G^2 |M|^2}{12\pi^4} \frac{1}{k} \left\{ \left[W_0^4 \left(\frac{2}{3} x^3 + x \right) + W_0^3 \left(-\frac{7}{3} x^4 - 3x^2 + \frac{1}{8} \right) + W_0^2 \left(\frac{18}{5} x^5 + 5x^2 \right) + W_0 \left(-\frac{13}{5} x^6 - \frac{14}{3} x^4 - \frac{15}{8} x^2 - \frac{5}{24} \right) + \left(\frac{76}{105} x^7 + \frac{5}{3} x^5 + \frac{11}{6} x^3 + \frac{3}{8} x \right) \right] ln[x + (x^2 - 1)^{1/2}] - \left[W_0^4 \left(\frac{11}{9} x^2 + \frac{4}{9} \right) + W_0^3 \left(-\frac{151}{36} x^3 - \frac{73}{72} x \right) + W_0^2 \left(\frac{163}{25} x^4 + \frac{152}{75} x + \frac{4}{75} \right) + W_0 \left(-\frac{4303}{900} x^5 - \frac{5783}{1800} x^3 - \frac{2441}{1800} x \right) + \left(\frac{14,741}{11,025} x^6 + \frac{8133}{4900} x^4 + \frac{135,853}{88,200} x^2 + \frac{136}{2205} \right) \right] (x^2 - 1)^{\frac{1}{2}} \right\} \quad (7)$$

IB spectrum in tensor interaction for isotopes with first forbidden beta transitions is;

$$S(k) = \frac{\alpha G^2 |M|^2}{12\pi^4} \frac{1}{k} \left\{ \left[W_0^4 \left(\frac{2}{3} x^3 + x \right) + W_0^3 \left(-2x^4 - 2x^2 + \frac{1}{4} \right) + W_0^2 \left(\frac{43}{15} x^5 + \frac{8}{3} x^3 - \frac{3}{8} x \right) + W_0 \left(-\frac{31}{15} x^6 - \frac{7}{3} x^4 - \frac{3}{8} x^2 - \frac{1}{12} \right) + \left(\frac{64}{105} x^7 + \frac{8}{5} x^5 + \frac{1}{12} x \right) \right] ln \left(x + (x^2 - 1)^{1/2} \right) - \left[W_0^4 \left(\frac{11}{9} x^2 + \frac{4}{9} \right) + W_0^2 \left(-\frac{7}{2} x^3 - \frac{1}{4} x \right) + W_0^2 \left(\frac{4481}{900} x^4 + \frac{97}{600} x^2 + \frac{4}{225} \right) + W_0 \left(-\frac{363}{100} x^5 - \frac{1337}{1800} x^3 - \frac{437}{900} x \right) + \left(\frac{1306}{1225} x^6 - \frac{769}{22,050} x^4 + \frac{7733}{44,100} x^2 + \frac{24}{1225} \right) \right] (x^2 - 1)^{\frac{1}{2}} \right\}. \quad (8)$$

Where, G is a constant that determines the strength of the coupling of the electron neutrino field with nuclei. M is the matrix element. α is the fine structure constant with a value of 1/137, W_0 is the total energy in the rest mass energy unit and k is the energy value of the photon.

3. Results and Discussion

The radionuclide $^{86}_{37}$Rb has a branch with two different maximum energies. The first branch decay into the ground level of (2-> 0+) transition having an $E_{m1} = 1774.4$ keV endpoint energy and a decay probability of $\eta1 = 0.912$. This transition is classified as a unique first-forbidden transition. The other branch, decays into the first excited state of (2- > 2+) transition having an $E_{m2} = 697.0$ keV endpoint energy and a $\eta2 = 0.088$ disintegration probability. This forbidden transition state is labeled as the first non-unique. IB calculations with KUB theory were performed separately for the two decay branches. In order to obtain the total spectrum, the decay rates of the respective decay branches were added together.

IB spectra obtained for $^{86}_{37}$Rb radionuclide are given in Figure 2. Some abbreviations have been made for the spectra obtained in the given graph. Accordingly, MC specifies the Monte Carlo solution. For allowed transitions, LF and LF2 show, Z = 0 and Z ≠ 0 respectively, LF3 and LF4 show the IB spectra containing Coulomb corrections for the forbidden transitions in the case of Z = 0 and Z ≠ 0, respectively. Abbreviations for SCA and TNS show the IB spectrum solutions for forbidden transitions by Bolgiano et al. [14]. Finally, the abbreviation KUB represents the IB spectrum obtained by the analytical solution given by Chang and Falkoff [10].
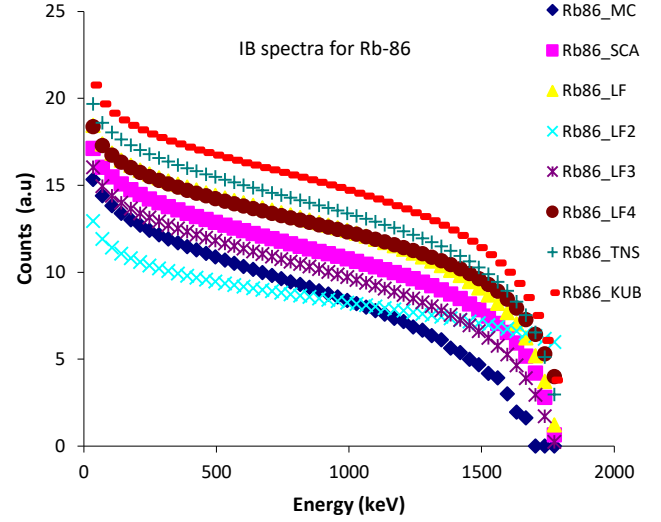

Figure 2. IB spectra obtained by the solutions from the Monte Carlo Method, KUB theory, tensor and scalar calculations for forbidden transition and Coulomb corrected allowed and forbidden transition for $^{86}_{37}$Rb

All solutions given are parallel to each other except for the LF2 solution. In the high energy region, the MC solution drops faster than other solutions. While the LF and LF4 are very compatible with each other, the LF4 solution deviated slightly upwards in the region from 1200 keV to endpoint energy. KUB, TNS and SCA solutions have been parallel to each other.

4. Conclusions

Within the framework of these graphical data, the phenomenon of internal bremsstrahlung released into the environment by the sudden change of nuclear charge during beta disintegration due to bremsstrahlung event, which is an important issue in nuclear physics, was examined in this study with theoretical and Monte Carlo method. We compared the IB spectra from theoretical calculation to the IB spectrum by Monte Carlo method for the Rb-86 isotope. In the comparison, we took into account the agreements in low energy, medium energy and high energy regions. When we look at IB studies historically, positive deviations in experimental values between experimental and theoretical values always occur especially in high energy region. The value of this study is that the IB spectrum can be predicted by the Monte Carlo method as well as the theoretical calculations and the option of comparing it with the experimental data can be presented.

References

[1] Konopinski, E.J. 1966. The Theory of Beta Radioactivity, Oxford University Press, London

[2] Wu, C.S., S.A. Moskowski. 1966. Beta Decay, Wiley, New York.

[3] Parker, S.P.,(Editor).1983. Encyclopedia of Physics, McGraw-Hill, New York.

[4] Evans, R.D. 1955. The Atomic Nucleus, McGraw-Hill, New York.

[5] Almaz. E. 2000. The Investigation of Internal Bremsstrahlung Spectra of β^- Particles. Master of Science Thesis. Institute of Science, Uludağ University, Bursa.

[6] Knipp, J.K., Uhlenbeck, G.E., 1936. Emission of gamma radiation during the beta decay of nuclei, Physica, 3, 425-439.

[7] Bloch, F., 1936, On the continuous γ-radiation accompanyig the β-decay, *Physical Review,* 50 (1), 272-279.

[8] Chang, C.S.W., Falkoff, D.L., 1949, On the continuous gamma-radiation accompanying the beta-decay of nuclei, *Physical Review*, 76, 365-372.

[9] Nilsson, S.B., 1956. On the Coulomb effect for the internal bremsstrahlung accompanying beta decay. Ark. Fys. 10, 467–477.

[10] Lewis, P.R., Ford, G.W., 1957, Coulomb effects in inner bremsstrahlen. *Physical Review*, 107 (3), 756-765.

[11] Spruch, L., Gold, W., 1959, Coulomb corrections in the theory of internal bremsstrahlung, *Physical Review*, 113, 1060-1069.

[12] Ford, G.W., Martin, C.F., 1969. Detour transitions in internal bremsstrahlung. Nucl. Phys. A 134, 457–469.

[13] Cengiz, A., Almaz, E., 2004, Internal bremsstrahlung spectra of $\beta-$ particle emitters using the Monte Carlo method, *Radiation Physics and Chemistry*, Bursa, 70, 661-668

[14] Bolgiano, P., Madansky, L., Rasetti, F., 1953, The Continuous Gamma-Ray Spectrum Accompanying Beta-Decay, *Physical Review,* 89, 679-684.

[15] Rubinstein, R.Y., 1981, Simulation and the Monte Carlo Method, John Wiley and Sons, *New York*, 71-166.

Effects of commonly used pesticides (demond, granland and safacol) on non-targeted organisms (wheat plant, soil nematodes, microfungi and aerobic mesophilic bacteria) in Muş Province, Turkey

İbrahim Koç [a,*] (ID), Emrullah Urgan [a] (ID), Ayşenur Güven [a] (ID), Birgül Ilıkhan [b] (ID)

[a] Bitlis Eren University, Department of Environmental Engineering, TR-13000, Bitlis Turkey

[b] Bitlis Eren University, Department of Biology, TR-13000, Bitlis Turkey

ARTICLE INFO

ABSTRACT

Chemical drugs (pesticides) that are xenobiotic to the nature of agricultural agro-ecosystems affect the target organism and non-target factors. The efficiency and reliability of agricultural areas are important not only for living creatures in the environment, but also for community. This study was carried out to determine the effects of Demond EC 2.5 (insecticide), Granland DF (herbicide) and Safacol 70 WP (fungicide) pesticides, which are widely used in the agricultural areas of Muş, on the development of non-target wheat plant, free-living nematodes, microfungi and aerobic mesophilic bacteria communities. The study was performed in three replicates in the variance analysis method for repeated measurements in laboratory conditions. Pesticides were applied by spraying to the pots including one kg of soil as recommended and upper doses, respectively, with the help of an injector. Repeated Measurement ANOVA and Profile Analysis Technique were used in the comparison of treatments in terms of nematode, bacteria and microfungi numbers (before-after), and the Analysis of Means (ANOM) Technique in comparing treatments in terms of plant parameters. As a result of the experiments; While the effect of only periods is important for the bacteria combination (P=0.001); for the microfungi community, both period (P=0.004) and Period × Treatment interaction were found significant (P=0.050). Periodic × Treatment interaction was statistically significant for plant-parasitic, omnivore-predator, bacterivore and total nematodes respectively (P=0.002; P=0.004; P=0.001; P=0.000). As a result; the pesticides used had more or less positive effects on the microfungi community, while they had a negative effect on the bacteria community; According to trophic levels, soil nematodes and plant parameters were found to have a positive / negative effect. It is thought that pesticides should be used in the last resort and recommended dosage, without forgetting that the soil is complex and all living things share this environment.

1. Introduction

Agro-ecosystems are complex environments and the activities carried out here affect productivity, as well as sustainability, environmental and human health. Manufacturers prefer using chemical pesticides to get more crops from agricultural areas. In this context, Özbek and Fidan (2014), although the differences from time to time, between 1979 to 2007 pesticide use increased by 270% in Turkey. Quinn et al. (2011) reported that although the benefit provided by pesticides cannot be denied, the negativities it gives to the environment and human

* Corresponding author.
  Tel.: +0 505 477 1198; fax: +0 000 000 0000
  E-mail address: ibrahimkoc47@gmail.com
  ORCID : 0000-0003-0803-6801 *(İbrahim KOÇ)*, 0000-0003-0131-3052 *(Emrullah URGAN)*, 0000-0002-0976-7545 *(Ayşenur GÜVEN)*,
    0000-0003-4629-1192 *(Birgül ILIKHAN)*

health cannot be ignored. The indiscriminate use of pesticides affects soil microflora, fauna and flora (Arora et al., 2019). AL-Ani et al. (2019) reported that pesticides, in which they applied different doses, negatively affect the microbial activities of bacteria, microfungi and actinomycetes in the soil, and significantly reduced their number. Ekundayo (2003) found that among the pesticides treated to the garden soil at the recommended doses, Agrosan is the most negative pesticide affecting bacteria density. Ubuoh et al. (2012) observed that glyphosphate treatments caused a significant reduction in microfungi and bacteria population compared to control. Ören et al. (2009) stated that the pesticides they use show different effects on bacteria and yeast-molds in the soil. Demirci et al. (2002) have listed the fungicides they use against fungi to be effective (Flusilazole, Tebuconazole, Diniconazole, Penconazole, Cyproconazole, Triticonazole). Arora and Sahni (2016) reported that microorganisms react differently to different pesticides. Heinonen-Tanski et al. (1989) reported that soil microorganisms were affected by pesticides used in their studies in some cases, but not in all cases. Lo (2010) stated that pesticides have different effects against soil microorganisms due to their different structure. Küçük et al. (2009) concluded that some fungicides may negatively affect the development of fungal isolates (*T. harzianum*, a biocontrol factor). Koç and Yardım (2019) reported that the pesticides (herbicides and fungicides) they used did not significantly affect soil microfungi and aerobic mesophilic bacteria density. Güven and Koç (2020a) found that the bacteria population in the pesticide treated samples compared to the control treatment showed a decrease in other treatments, while the microfungi population increased only in the treatment of Pesos 100 EC. Wesley et al. (2017), they observed that different results were obtained according to the parameters considered.

Arora and Sahni (2016) predicted that chemical pesticides disrupt the activities of soil microorganisms and therefore the nutritional quality of the soil may be affected, and this situation may lead to serious ecological consequences. Küçük et al. (2016) reported that it is inevitable to use fungicides in the fight against pest and therefore it should be used considering the effect of the fungicides to be used on soil microorganisms. Johns (2017) stated that soil microbiology should be better understood in order for agricultural production to meet the needs of the growing world population. Yardim and Edwards (1998) stated that nematodes (according to trophic groups) respond positively / negatively to pesticides used in field trials. Daramola et al. (2015) reported that Carbofuran's nematode population was significantly suppressed. Römbke et al. (2009) stated that the pesticides they used reduced the number of nematodes by 48% compared to the control. Koç et al. (2020), according to their compliance analysis, found significant relationships between pesticide treatments and nematode groups. Güven and Koç (2020b) declared that the pesticides they use affect soil nematodes. Demircioğlu (2007) stated that herbicides tested in different environments and shapes affect the number of seed germination, sugar beet wet, dry and root weight. Fındıklı and Türkoğlu (2010) found that all doses of pesticides they use have an inhibitory effect on cell division at the root ends of *Allium cepa*. Sıddıqı and Ahmed (2006) observed that the pesticide concentrations they use have combined effects on plant growth and the nutritional

composition of seeds. Niewiadomska and Klama (2005) have demonstrated that the pesticides they apply have a toxic effect on the nodulation and root growth of the tested plants. Boutin et al. (2014) stated that as a result of the use of pesticides, a large number of non-targeted plants and vegetation have changed significantly, in addition, there is a delay in flowering and a decrease in seed production. Ilıkhan and Koç (2020) reported that Demond EC 2.5 and Safacol 70 WP had a toxic effect on *E. fetida*. This study was conducted for the purpose of determining the effects of Demond EC 2.5 (insecticide), Granland DF (herbicide) and Safacol 70 WP (fungicide), which are widely used in agricultural areas of the province of Muş, Turkey on the free-living nematodes, microfungi and aerobic mesophilic bacteria communities.

2. Material and Methods

This study was carried out in in-vitro conditions (mean temperature: 23 °C) between 2019-2020. The soil used in the study is from the pasture environment (Latitude: 38° 28'54.75'', Longitude: 42° 9'51.93'') and 0-30 cm depth (Yıldız et al., 2019) for the agricultural activities in the Bitlis Eren University Campus area. Taken on August 2, 2019. Samples were passed through a 2 mm sieve and kept in clean nylon bags at +4 °C in the refrigerator until experimenting. Soil texture, according to Bouyoucos (1951) (clay ratio; 32%, silt ratio; 5%, sand ratio; 63%, lime ratio; 1.43%, pH; 7.8, EC; 181 µS/cm^{-1}); Moisture content (%) was determined before and after treatment (12.7%, 14.6%) according to Craze (1990). For 2017, pesticides commonly used in the province of Muş were determined by asking the Muş Provincial Directorate of Agriculture and Forestry, pesticides and farmers. A total of three [Demond EC 2.5 (insecticide, Deltamethrin 25 g/l active substance), Granland DF (herbicide, 75% Tribenuron-methyl) and Safacol 70 WP (fungicide, 70% Propineb)] were used to represent the pesticide groups. Trial measurements were carried out in three replications according to the variance analysis method (Figure 1). Before the pesticide treatment, Ceyhan-99 bread wheat seeds (twenty piece) were planted 3 cm deep. Determined pesticides were used with the help of injector (5 cc) as twice the recommended dose and the recommended dose. Demond EC 2.5 (200 ml distilled water + 0.1 ml drug; 200 ml distilled water + 0.2 ml drug), Granland DF (150 ml distilled water + 0.02 mg drug; 150 ml distilled water + 0.04 mg drug), and Safacol 70 WP (200 ml of distilled water + 0.5 g of drug; 200 ml of distilled water + 1 g of drug) was prepared by spraying 50 ml of solution (distilled water + drug) into pots placed in a kg of soil.

Figure 1. Sample image from trial.

The average sprouting time of the seeds was 4 days. After sprouting, 10 plants were left in each pot. The experiment lasted about a month (January 7 – February 3, 2019) and soil samples were taken before and after pesticide treatment, according to nematode counts (trophic groups), microfungi, and aerobic mesophilic bacteria were examined. The determination of the total number of microfungi and aerobic mesophilic bacteria was done according to Benson (2001). Plate Count Agar for bacteria count and Rose Bengal-chloramphenicol Agar media were used for microfungi count. For extraction and counting of nematodes, "Improved-Baermann Funnel Method" according to was used (Baermann, 1917; Whitehead and Hemming, 1965; Southey, 1986), the microscope's lens (×10) counts according to Yeates (1971) and Yeates et al. (1993). The dismantling process was removed from the soil by carefully washing it thoroughly with water after the soil in the pots was removed together with the plants. For each pot, five randomly selected plants were taken to represent the whole of the cleaned plants, and measurements were made. Wheat plants root length (cm), seedling length (cm), root weight (g), seedling weight (g), dry root weight (g), dry seedling weight (g), dry root/seedling ratio and root volume (cm^3) measurements (Geçit et al., 1987; Sönmez, 2001; Sipan, 2014). In the investigation of the effects of pesticide treatments (before and after treatment), Repeated Measured Variance Analysis and Profile Analysis Techniques were used to compare the treatments in terms of plant parameters (ANOM) Technique (Mendeş et al., 2007; Mendeş, 2012). SPSS (ver. 19.0) and Minitab (ver. 17) statistical package programs were used in making statistical analyzes.

3. Results and Discussion

3.1. Effect of pesticide treatments on soil-free nematodes

3.1.1. Effect of treatments on plant-parasitic nematode count

According to the repeatedly measured variance analysis on the data obtained, the Period × Treatment interaction effect was found statistically significant (P=0.002). In other words, the effect of pesticide treatments on the number of plant-parasitic nematodes varied significantly in periods (Table 1).

Table 1. Introductory statistics in terms of plant-parasitic nematode number.

Pesticide Treatments	N	Before Treatment $\overline{X} \pm S_{\overline{x}}$	After Treatment $\overline{X} \pm S_{\overline{x}}$
Demond recommended d.	3	2.00±0.47	7.33±0.90
Demond a single high d.	3	9.67±0.67	3.33±0.60
Granland recommended d.	3	8.00±0.94	4.33±0.69
Granland a single high d.	3	16.00±1.33	3.67±0.64
Safacol recommended d.	3	8.00±0.94	11.00±1.10
Safacol a single high d.	3	4.67±0.72	5.67±0.79
Control	3	15.00±1.29	4.33±0.69
Total	21	9.05±1.00	5.67±0.79

When the results of the profile analysis are examined, the granland did not affect any toxic effect, except for the relative negative in the recommended dose. Even, it has been determined that demond has a positive effect on the increase in the number of plant-parasitic nematodes in recommended doses and safacol treatments (Table 1, Figure 2).
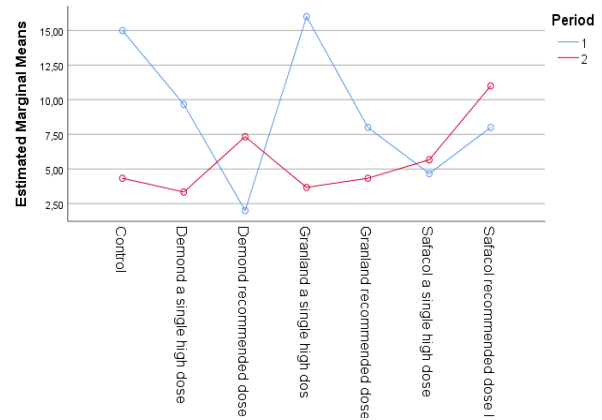

Figure 2. Profile analysis in terms of plant-parasitic nematode number.
* Period 1: Before treatment, Period 2: After treatment

3.1.2. Effects of treatments on fungivore nematode count

As a result of repeated measured variance analysis on the obtained data, the Period × Treatment interaction effect was not statistically significant (P=0.265). Therefore, the effect of pesticide treatments on fungivore nematode numbers did not change significantly according to periods (Table 2).

Table 2. Effects of treatments on fungivore nematode count.

Pesticide Treatments	N	Before Treatment $\overline{X} \pm S_{\overline{x}}$	After Treatment $\overline{X} \pm S_{\overline{x}}$
Demond recommended d.	3	3.00±0.57	2.33±0.51
Demond a single high d.	3	2.67±0.54	2.00±0.47
Granland recommended d.	3	5.00±0.74	2.33±0.51
Granland a single high d.	3	5.67±0.79	4.00±0.67

Safacol recommended d.	3	2.67±0.54	2.00±0.47
Safacol a single high d.	3	5.33±0.77	2.33±0.51
Control	3	2.67±0.54	8.00±0.94
Total	21	3.86±0.65	3.29±0.60

When the results of the profile analysis on the data are examined; according to the control, all pesticide treatments seem to have a negative effect on fungivore nematodes (Table 2, Figure 3).
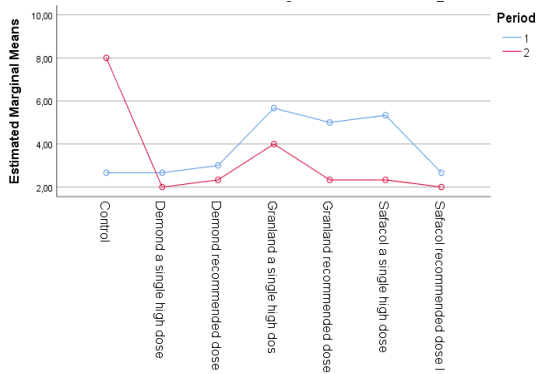
Figure 3. Profile analysis in terms of the number of fungivore nematodes.
* Period 1: Before treatment, Period 2: After treatment

3.1.3. The effect of treatments on the number of bacterivore nematodes

As a result of repeated measured variance analysis, the Period × Treatment interaction effect was found statistically significant (P=0.001). Therefore, the effect of pesticide treatments on the number of bacterivore nematodes varied significantly over periods (Table 3).

Table 3. Introductory statistics in terms of bacterivore nematode number.

Pesticide Treatments	N	Before Treatment	After Treatment
		$\overline{X} \pm S_{\overline{x}}$	$\overline{X} \pm S_{\overline{x}}$
Demond recommended d.	3	13.33±1.22	16.33±1.35
Demond a single high d.	3	9.33±1.02	18.00±1.41
Granland recommended d.	3	20.67±1.51	9.00±1.00
Granland a single high d.	3	19.33±1.46	10.33±1.07
Safacol recommended d.	3	10.67±1.09	19.67±1.48
Safacol a single high d.	3	8.00±0.94	27.67±1.75
Control	3	27.33±1.74	41.00±2.13
Total	21	15.52±1.31	20.29±1.50

Looking at the results of profile analysis; according to the control, it was observed that especially granland had a negative effect on bacterivore nematodes (Table 3, Figure 4).
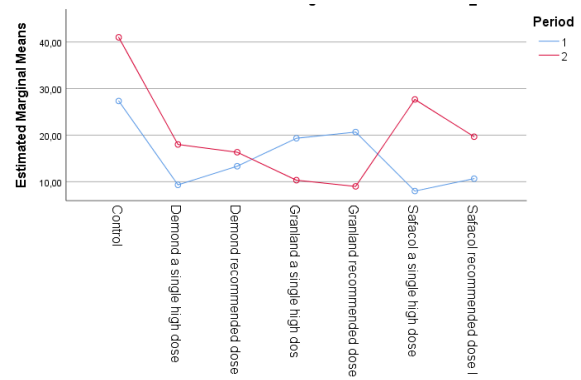
Figure 4. Profile analysis in terms of bacterivore nematode count.
* Period 1: Before treatment, Period 2: After treatment

3.1.4. The effects of treatments on the number of omnivore-predator nematodes

As a result of repeated measured variance analysis, the Period × Treatment interaction effect was found statistically significant (P=0.004). In other words, the effect of pesticide treatments on the number of omnivore-predator nematodes varied significantly in periods (Table 4).

Table 4. Introductory statistics in terms of the number of omnivore-predator nematodes.

Pesticide Treatments	N	Before Treatment	After Treatment
		$\overline{X} \pm S_{\overline{x}}$	$\overline{X} \pm S_{\overline{x}}$
Demond recommended d.	3	3.67±0.64	9.33±1.02
Demond a single high d.	3	3.67±0.64	9.67±1.04
Granland recommended d.	3	10.67±1.09	8.67±0.98
Granland a single high d.	3	6.67±0.86	8.00±0.94
Safacol recommended d.	3	4.67±0.72	11.00±1.10
Safacol a single high d.	3	4.67±0.72	19.33±1.46
Control	3	13.33±1.22	27.33±1.74
Total	21	6.76±0.87	13.33±1.22

Looking at the results of profile analysis; according to the control, it was found that demond and granland had negative effects on omnivore-predator nematodes (Table 4, Figure 5).
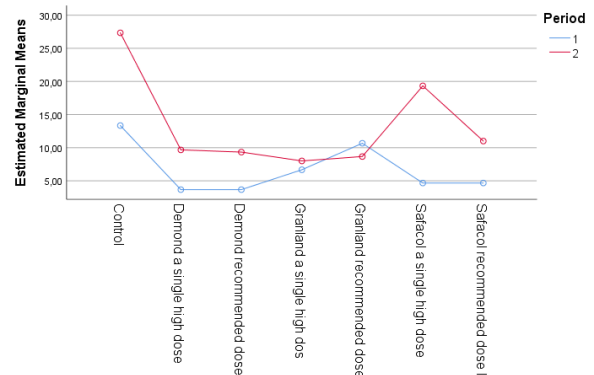
Figure 5. Profile analysis in terms of number of omnivore-predator nematodes.
* Period 1: Before treatment, Period 2: After treatment

3.1.5. The effects of treatments on the total number of nematodes

As a result of repeated measured variance analysis, the Period × Treatment interaction effect was found statistically significant (P=0.000). Therefore, the effect of pesticide treatments on the total number of nematodes varied significantly over periods (Table 5).

Table 5. Introductory statistics in terms of total number of nematodes.

Pesticide Treatments	N	Before Treatment $\overline{X} \pm S_{\overline{x}}$	After Treatment $\overline{X} \pm S_{\overline{x}}$
Demond recommended d.	3	21.67±1.55	35.33±1.98
Demond a single high d.	3	25.33±1.68	33.00±1.91
Granland recommended d.	3	44.00±2.21	24.33±1.64
Granland a single high d.	3	47.33±2.29	26.00±1.70
Safacol recommended d.	3	26.00±1.70	43.67±2.20
Safacol a single high d.	3	22.67±1.59	55.00±2.47
Control	3	58.00±2.54	80.67±3.00
Total	21	35.00±1.97	42.57±2.17

Looking at the results of profile analysis; according to the control, it was observed that especially granland had a negative effect on total nematodes (Table 5, Figure 6).
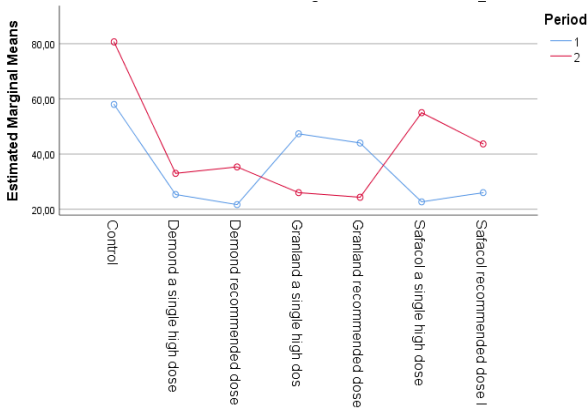

Figure 6. Profile analysis in terms of total number of nematodes.
* Period 1: Before treatment, Period 2: After treatment

3.2. Effect of pesticide treatments on soil microorganisms

3.2.1. The effects of treatments on the number of aerobic mesophilic bacteria

As a result of repeated measured variance analysis, the Period × Treatment interaction effect was not found statistically significant (P=0.835). Therefore, the effect of pesticide treatments on aerobic mesophilic bacteria number did not change significantly according to periods (Table 6).

Table 6. Introductory statistics in terms of the number of aerobic mesophilic bacteria.

Pesticide Treatments	N	Before Treatment $\overline{X} \pm S_{\overline{x}}$	After Treatment $\overline{X} \pm S_{\overline{x}}$
Demond recommended d.	3	1766666.67±443.05	22333333.33±1575.27
Demond a single high d.	3	15666666.67±1319.37	25000000.00±1666.67
Granland recommended d.	3	18000000.00±1414.21	32333333.33±1895.41
Granland a single high d.	3	8000000.00±942.81	26000000.00±1699.67
Safacol recommended d.	3	3333333.33±608.58	14666666.67±1276.57
Safacol a single high d.	3	3200000.00±596.28	30333333.33±1835.86
Control	3	766666.67±291.86	33666666.67±1934.10
Total	21	7247619.05±897.38	26333333.33±1710.53

When the profile analysis results are examined, it has been found that pesticide treatments have more or less negative effects on the number of aerobic mesophilic bacteria compared to the control (Table 6, Figure 7).
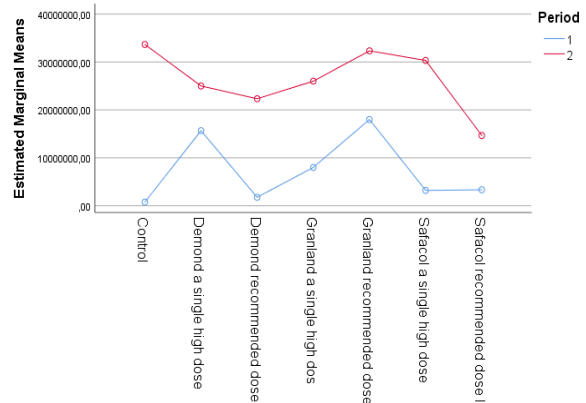

Figure 7. Profile analysis in terms of the number of aerobic mesophilic bacteria.
* Period 1: Before treatment, Period 2: After treatment

3.2.2. The effect of treatments on the number of microfungi

As a result of repeated measured variance analysis, the Period × Treatment interaction effect was found statistically significant (P=0.050). Therefore, the effect of pesticide treatments on the number of microfungi varied significantly in periods (Table 7).

Table 7. Introductory statistics in terms of microfungi number.

Pesticide Treatments	N	Before Treatment	After Treatment
		$\overline{X} \pm S_{\overline{x}}$	$\overline{X} \pm S_{\overline{x}}$
Demond recommended d.	3	2333.33 ± 16.10	4700.00 ± 22.85
Demond a single high d.	3	2400.00 ± 16.33	3666.67 ± 20.18
Granland recommended d.	3	2333.33 ± 16.10	3600.00 ± 20.00
Granland a single high d.	3	3533.33 ± 19.81	4366.67 ± 22.03
Safacol recommended d.	3	1733.33 ± 13.88	3700.00 ± 20.27
Safacol a single high d.	3	3600.00 ± 20.00	3766.67 ± 20.46
Control	3	4833.33 ± 23.17	3533.33 ± 19.81
Total	21	2966.67 ± 18.15	3904.76 ± 20.83

When the profile analysis results were examined, it was found that pesticide treatments had more or less positive effects on the number of microfungi according to the control (Table 7, Figure 8).
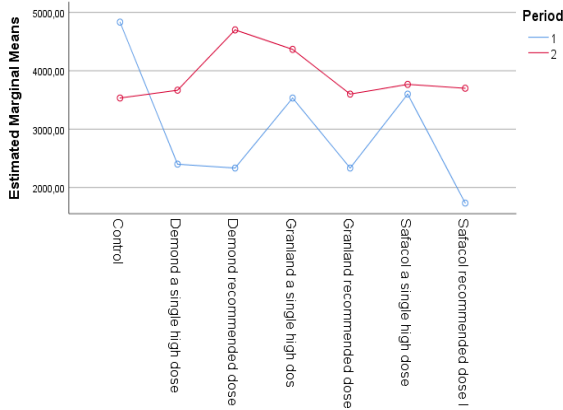

Figure 8. Profile analysis in terms of microfungi number.
* Period 1: Before treatment, Period 2: After treatment

3.3. The effect of pesticide treatments on the development of root and above-ground parts in the first development period of wheat

3.3.1. Effect of treatments on plant root length (cm)

According to the ANOM test performed in terms of the effect of pesticide treatments on plant root length, it was observed that safacol had a positive effect and granland had a negative effect compared to the control (Figure 9).
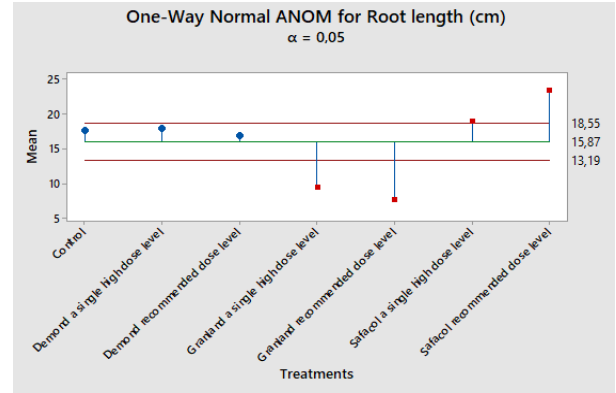

Figure 9. ANOM graphic in terms of plant root length.

3.3.2. Effect of treatments on plant shoot length (cm)

According to the ANOM test conducted in terms of the effect of pesticide treatments on plant shoot length, it was found that demond had a positive effect and granland had a negative effect when compared with the control (Figure 10).
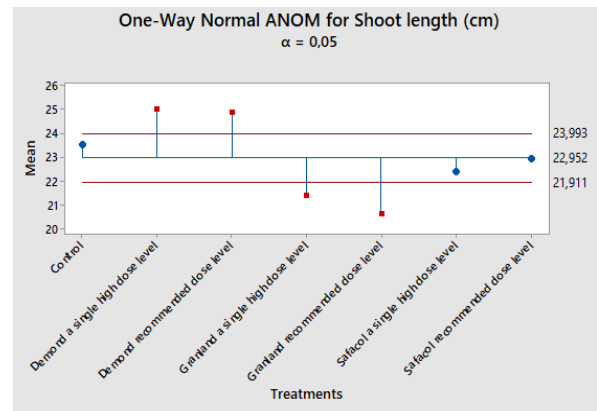

Figure 10. ANOM graphic in terms of plant shoot length.

3.3.3. Effect of treatments on plant root weight (g)

According to the ANOM test results in terms of the effect of pesticide treatments on plant root weight, it was found that other treatments that granland had a positive effect compared to the control had a relatively positive effect (Figure 11).
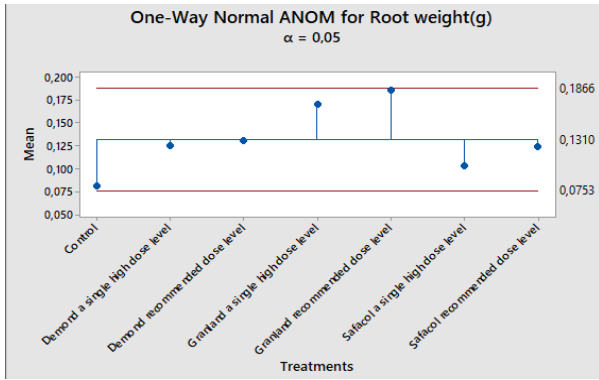
Figure 11. ANOM graphic in terms of plant root weight.

3.3.4. Effect of treatments on plant shoot weight (g)

According to the ANOM test performed in terms of the effect of pesticide treatments on plant shoot weight, safacol was found to be positive while other treatments had a positive effect compared to the control (Figure 12).
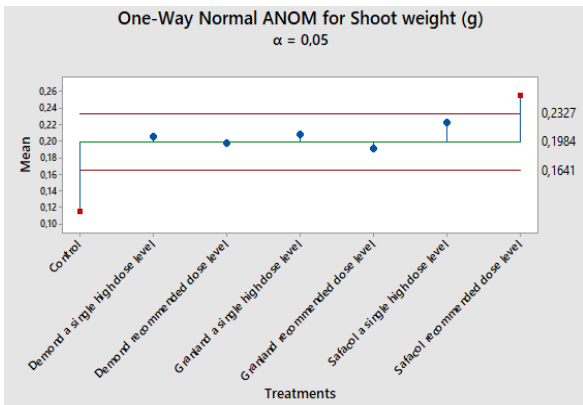

Figure 13. ANOM graphic in terms of plant dry root weight.

3.3.6. Effect of treatments on plant dry shoot weight (g)

According to the ANOM test performed in terms of the effect of pesticide treatments on plant dry shoot weight, compared to the control, safacol suggested overdose treatment positively and other treatments affected relatively (Figure 14).

Figure 12. ANOM graphic in terms of plant shoot weight.

3.3.5. Effect of treatments on plant dry root weight (g)

According to the ANOM test performed in terms of the effect of pesticide treatments on plant dry root weight, it was found to be relatively affected compared to the control (Figure 13).

Figure 14. ANOM graphic in terms of plant dry shoot weight.

3.3.7. Effect of treatments on plant dry root / shoot ratio

According to the ANOM test performed in terms of the effect of pesticide treatments on the plant dry root / shoot ratio, it was observed that all treatments were relatively affected when compared with the control (Figure 15).
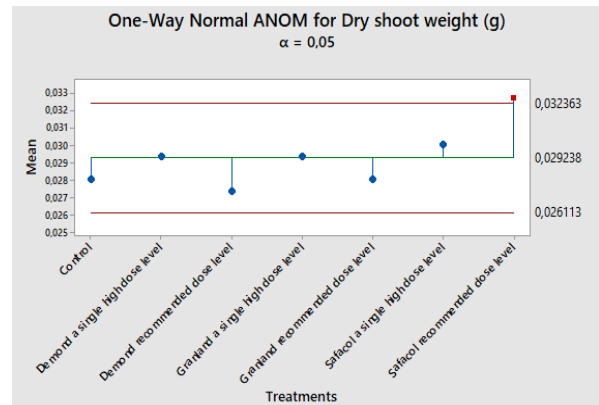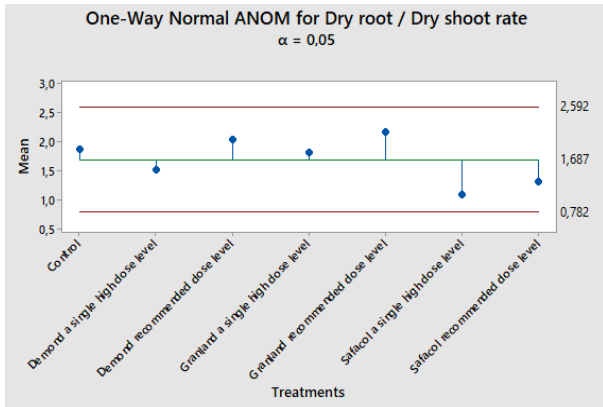
Figure 15. ANOM graphic in terms of plant dry root / shoot ratio.

3.3.8. Effect of treatments on plant root size (cm³)

According to the ANOM test results in terms of the effect of pesticide treatments on plant root size, all pesticide treatments were found to be partially effective compared to the control (Figure 16).
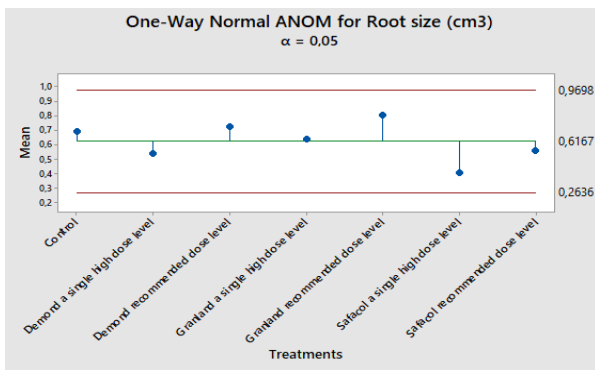

Figure 16. ANOM graphic in terms of plant root size (cm³).

Chemical drugs (pesticides) used in disease, pest and weed control not only affect the target parameter, but unfortunately also affect the biotic and abiotic parameters that are not targeted and whose assets are indisputably indispensable. Treatments performed in this study showed positive, negative and neutral effects compared to the control and dosage used in terms of plant growth parameters. The results obtained in this study were partially in agreement with Demircioğlu (2007), Fındıklı and Türkoğlu (2010), Sıddıquı and Ahmed (2006), Niewiadomska and Klama (2005) and Boutin et al. (2014). As free-living nematodes in soil, grandland, which is one of the pesticide treatments, generally shows toxic effects; with the recommended dose of demond, safacol has also been found to have a positive effect on plant-parasitic nematodes and other treatments have different effects. Further, similar outcomes with previous studies including Yardim and Edwards (1998), Römbke et al. (2009) and Koç et al. (2020) were obtained in the laboratory experiments. When evaluated in terms of microfungi; the treatments were found to have more or less positive effects on the number of microfungi. Although some of

the findings in this study were contrary to the suggestions proposed by AL-Ani et al. (2019), Ubuoh et al. (2012) and Küçük et al. (2009), they were substantially consistent with Wesley et al. (2017), Arora and Sahni (2016), Arora et al. (2019), Ören et al. (2009), Heinonen-Tanski et al. (1989) and Koç and Yardım (2019). In terms of aerob mesophilic bacteria, pesticides were found to have more or less toxic effects. The findings of this study were relatively parallel with Ubuoh et al. (2012), Güven and Koç (2020a) and AL-Ani et al. (2019, Ören et al. (2009), Ekundayo (2003), Heinonen-Tanski et al. (1989), Yousaf et al. (2013), Lo (2010), Arora and Sahni (2016), Aries and Aid (2019) and Wesley et al. (2017). Based on the findings obtained, different results (such as positive, negative and neutral) were obtained, depending on the type and dose of the drug used and the parameter considered. It is thought that this situation may be caused by the variability of factors such as the type of drug used, dosage, parameter taken into account and the environment studied.

As a result; It can be stated that the negative effects of pesticides to the environment cannot be ignored (Quinn et al., 2011; Arora and Sahni, 2016; Küçük et al., 2016) and soil microbiology should be better understood in order for agricultural production to meet the needs of the growing world population (Johns, 2017).

Acknowledgements

References

AL-Ani, M.A., Hmoshi, R.M., Kanaan, I.A., and Thanoon, A.A., 2019. Effect of Pesticides on Soil Microorganisms. In Journal of Physics: Conference Series (Vol. 1294, No. 7, p. 072007). IOP Publishing

Arora, S., and Sahni, D., 2016. Pesticides Effect on Soil Microbial Ecology and Enzyme Activity-An Overview. Journal of Applied and Natural Science, 8(2), 1126-1132.

Arora, S., Arora, S., Sahni, D., Sehgal, M., Srivastava, D.S., and Singh, A., 2019. Pesticides Use and Its Effect on Soil Bacteria and Fungal Populations, Microbial Biomass Carbon and Enzymatic Activity. Curr Sci, 116(4), 643-649.

Baermann, G., 1917. Eine einfache Methode zur Auffindung von Ancylostomum (Nematoden) Larven in Erdproben. Geneeskd Tijdschr Ned Indie, 57, 131-137.

Benson, H.J., 2001. Microbiological Applications: A Laboratory Manual in General Microbiology. Harold J. Benson. USA: The McGraw–Hill Companies, pp. 203.

Boutin, C., Strandberg, B., Carpenter, D., Mathiassen, S.K., and Thomas, P.J., 2014. Herbicide Impact on Non-Target Plant Reproduction: What are the Toxicological and Ecological Implications? Environmental Pollution, 185, 295-306.

Bouyoucos, G.J., 1951. A Calibration of the Hydrometer Method for Making Mechanical Analyses of Soils. Agronomy Journal, 43, 434-438.

Craze, B., 1990. Soil Survey Standard Test Method Soil Moisture Content. Department of Sustainable Natural Resources, 1-5.

Daramola, F., Afolami, S., Enikuomehin, O., Omonhinmin, C.A., Adebayo, H.A., 2015. Nematicidal Effects of Carbofuran and GC-MS Analysis of Its Residue in Pineapple Fruits. International Journal of Agriculture and Biology, 2, 357-362.

Demirci, A., Katırcıoğlu, Y. Z., Demirci, F., 2002. Investigations on the effects of triazole group fungicides on some important antagonistic fungi and non-pathogen *Fusarium oxysporum* (Schlecht) *in vitro*. Plant Protection Bulletin, 42(1-4), 53-65.

Demircioğlu, A., 2007. Determination of the Phytotoxic Effects of Some Herbicides Used on Corn to Sugarbeet (Ph. D. Thesis). Ankara University, Graduate School of Natural and Applied Sciences Department of Plant Protection, p.55, Ankara.

Ekundayo, E.O., 2003. Effect of Common Pesticides Used in The Niger Delta Basin of Southern Nigeria on Soil Microbial Populations. Environmental Monitoring and Assessment, 89(1), 35-41.

Findikli, Z., and Türkoğlu, Ş., 2010. The Effects of Glyphos and DDVP on Mitotic Division and Chromosomes in *Allium cepa* L. *J Sci Cumhuriyet Univ,*, 31(2), 49-62.

Geçit, H.H., Emeklier, H.Y., Çiftçi, C.Y., Ünver, S., and Şenay, A., 1987. Ekmeklik Buğdayda İlk Gelişme Devresinde Kök ve Toprak Üstü Organların Durumu. Türkiye Tahıl Sempozyumu, 6-9 Ekim 1987, Uludağ Üniversitesi Ziraat Fakültesi, Bursa.

Güven, A., and Koç, İ., 2020a. The Effects of Satellite 20 WP, Status 330 E, Pesos 100 EcC and Pentran 22 E Pesticides on Some Soil Parameters. 3.Uluslararasi Mardin Artuklu Bilimsel Araştirmalar Kongresi, 143-144, 18-19 Ocak 2020, Mardin.

Güven, A., and Koç, İ., 2020b. Investigation of the Effects of Some Pesticides Commonly Used in Bitlis on Soil Nematodes. 3.Uluslararasi Mardin Artuklu Bilimsel Araştirmalar Kongresi, 149-150, 18-19 Ocak 2020, Mardin.

Heinonen-Tanski, H., Simojoki, P., Raininko, K., Nuormala, N., and Silvo, R., 1989. Effect of Annual Use of Pesticides on Soil Microorganisms and Sugar Beet Yields. Agricultural and Food Science, 61(1), 45-53.

Ilıkhan, B., and Koç, İ., 2020. Some Biological Parameters of *Eisenia fetida* (Savigny, 1826) in Pesticide-Applied Vermicompost. KSU J. Agric Nat, 23(2), 367-378.

Johns, C., 2017. Living soils: The Role of Microorganisms in Soil Health. Fut Direct Intl, 1-7.

Koç, İ., and Yardım, E.N., 2019. Investigation of the Effects of Pesticides and Wood Vinegar on Some Microbial and Physico-chemical Soil Parameters. KSU J. Agric Nat, 22(6), 896-904.

Koç, İ., Yıldız, Ş., and Yardım, E.N., 2020. Effect of Some Pesticides and Wood Vinegar on Soil Nematodes in a Wheat Agro-Ecosystem. KSU J. Agric Nat, 23(3), 621-633.

Küçük, Ç., Kıvanç, M., Kınacı, E., and Kınacı, G., 2009. *Trichoderma harzianum* İzolatlarının Şeker Pancarında Kullanılan Bazı Fungisitlere Duyarlılıklarının i*n vitro*'da Araştırılması. Elektronik Mikrobiyoloji Dergisi TR, 7(2), 8-12.

Küçük, Ç., Yeşilorman, D., and Cevheri, C., 2016. Effect of Some Fungicides on Soil Biological Activities in Laboratory Conditions. Adıyaman Üniversitesi Fen Bilimleri Dergisi, 6(2), 187-201.

Lo, C.C., 2010. Effect of pesticides on soil microbial community. Journal of Environmental Science and Health Part B, 45(5), 348-359.

Mendeş M., Dincer E., and Arslan E., 2007. "Profile Analysis and Growth Curve for Body Mass Index of Broiler Chickens Reared Under Different Feed Restrictions in Early Age", Archiv Fur Tierzucht-Archives of Animal Breeding, 4, 403-411.

Mendeş, M., 2012. Uygulamalı Bilimler için İstatistik ve Araştırma Yöntemleri. Kriter Yayınevi, İstanbul.

Niewiadomska, A., and Klama, J., 2005. Pesticide Side Effect on The Symbiotic Efficiency and Nitrogenase Activity of Rhizobiaceae Bacteria Family. Polish Journal of Microbiology, 54(1), 43-48.

Ören, A., Özbolat, K., and Dığrak, M., 2009. Effect of the Some Pesticides on Soil Microorganisms Which Commonly Used in Kahramanmaraş Region. KSU J. Agric Nat,12(1), 23-28.

Özbek, F.Ş., and Fidan, H., 2014. Pesticides Usage in Wheat Production: Case Study of Konya. KSU J. Agric Nat, 17(3), 13-18.

Quinn, L., de Vos, J., Fernandes-Whaley, M., Roos, C., Bouwman, H., Kylin, H., Pieters, R., and van den Berg, J., 2011. Pesticide Use in South Africa: One of the Largest Importers of Pesticides in Africa. InTech, 1, p. 49-96.

Römbke, J., Schmelz, R.M., and Knabe, S., 2009. Field Studies for the Assessment of Pesticides with Soil Mesofauna, in Particular Enchytraeids, Mites and Nematodes: Design and First Results. Soil Organisms, 81(2), 237–264.

Siddiqui, Z.S., and Ahmed, S., 2006. Combined Effects of Pesticide on Growth and Nutritive Composition of Soybean Plants. Pakistan Journal of Botany, 38(3), 721.

Sipan, S., 2014. Some Properties of Root and Shoot of Some Bread Wheat *(Triticum aestivum* L. Em. Thell.) Cultivars in the First Development Stage (Master Thesis), Van Yüzüncü Yıl University, Msc, Department of Field Crops, p. 53, Van.

Sönmez, F., 2001. Tir buğdayı hatlarında ilk gelişme devresinde kök ve toprak üstü organların durumu. Türkiye 4. Tarla Bitkileri Kongresi, 297-302, 17-21 Eylül 2001, Tekirdağ.

Southey, J. F., 1986. Extract of Meloidogyne Egg Masses. In: Southey JF (ed) Laboratory Methods for Work with Plants and Soil Nematodes. HMSO, London. 42-44 pp.

Ubuoh, E.A., Akhionbare, S.M.O., and Akhionbare, W.N., 2012. Effects of Pesticide Application on Soil Microbial Spectrum: Case Study-Fecolart Demonstration Farm, Owerri-West, Imo State, Nigeria. International Journal of Multidisciplinary Sciences and Engineering, 3(2), 34-39.

Wesley, B., Ajugwo, G., Adeleye, S., Ibegbulem, C., and Azuike, P., 2017. Effects of Agrochemicals (Insecticides) on Microbial Population in Soil. EC Microbiology, 8, 211-221.

Whitehead, A.G., and Hemming, J.R., 1965. A Comparison of Some Quantitative Methods of Extracting Small Vermiform Nematodes from Soil. Annuals of Applied Biology, 55, 25-38.

Yardim, E.N., and Edwards, C.A., 1998. The Effects of Chemical Pest, Disease and Weed Management Practices on The Trophic Structure of Nematode Populations in Tomato Agroecosystems. Applied Soil Ecology, 7(2), 137-147.

Yeates, G.W., 1971. Feeding Types and Feeding Groups in Plant and Soil Nematodes. Pedobiologia, 8, 173-79.

Yeates, G.W., T Bongers., de Goede R.G.M., Freckman, D.W., and Georgleva, S.S., 1993. Feeding Habits in Soil Nematode Families and Genera - An Outline for Soil Ecologists. Journal of Nematology, 25, 315-331.

Yıldız, Ş., Koç, İ., and Yardım, E.N., 2017. Investigation on Nematode Faunal Structures in Pastures of Muş Province. YYU J AGR SCI, 27(2), 197-203.

Yousaf, S., Khan, S., and Aslam, M.T., 2013. Effect of Pesticides on the Soil Microbial Activity. Pakistan Journal of Zoology, 45(4), 1063-1067.

Effect of deformation on gamow-teller strength and electron capture cross-section for isotopes of chromium

Asim Ullah[a]* [iD], M. Riaz[a] [iD], Jameel-Un Nabi[a] [iD], Mahmut Böyükata[b] [iD], Necla Çakmak[c] [iD]

[a] GIK Institute of Engineering Sciences and Technology, Swabi, KPK, Topi 23640, PAKISTAN,
[b] Kırıkkale University, Science and Arts Faculty, Physics Department, Kırıkkale, 71450, TURKEY,
[c] Karabük University, Science Faculty, Department of Physics, Karabük, 78050, TURKEY,

ARTICLE INFO

ABSTRACT

In this work, we explore the role of deformation parameter (β) on the calculated Gamow-Teller (GT) strength distributions and electron capture cross-sections (ECC) for 46,48,50Cr isotopes within the formalism of the proton neutron-quasi-particle random phase approximation (pn-QRPA). Three different β parameters were used in the present study. Two of them were calculated by using the interacting boson model (IBM) and the macroscopic-microscopic (Mac-mic) models. The third one is the experimental β values obtained by employing its relation with the experimental B(E2)↑ values. The GT strength distributions were widely dispersed among all the daughter states of the given isotopes. They were found to have inverse relation with β parameter i.e decreasing with increasing the β value. The ECC were computed as a function of β parameter and the results suggest that the calculated ECC decreased with decreasing value of the β for the selected cases.

I. Introduction

The death of stars is commonly known as called supernova explosion. Study of such phenomenon can be used to explore our Universe. The electron capture (EC) and β-decay are keys to decipher the mysterious mechanism of the late stages of stellar evolution [1]. These weak decay processes also play essential role in estimating the pre-supernova core composition as well as synthesis of neutron-rich (massive) nuclei [1-2]. The EC process lowers the electron degenerate pressure and eventually causes the core collapse of the massive star. Thus, the collapse began through EC on iron regime nuclei [3]. In the start of the collapse i.e. at low stellar densities ($\sim 10^{10}$ gcm^{-3}) and low temperature (0.3 – 0.8 MeV), when the Q value and chemical potential of electrons have comparable magnitudes, the EC rates are sensitive to associated GT strength. For higher values of temperature and densities, the chemical potential surpasses the Q value and then the EC rates are largely dictated by the total GT strength. Therefore, the computation of the EC rates and GT strength distribution in the stellar matter is essential requirement.

Fuller, Fowler, and Newman [1] performed the pioneering calculation by tabulating the weak interaction rates employing the independent-particle model (IPM) with the help of available experimental data for astrophysical applications. Weak rates were tabulated for nuclei in mass range $21 \leq A \leq 60$. Later large-scale shell-model (LSSM) [4] was utilized to improve $\beta^{\pm}$ decay, positron and electron capture rates with the help of calculated GT strength distributions for various nuclei in the mass range 45-65. Based on these revised weak interaction rates, the pre-supernova phases of heavy mass stars were investigated in Ref. [5]. It was concluded that GT strength distributions and EC rates for *fp*-shell nuclei have significant impact on the pre-supernova evolution of massive stars. In recent past the proton neutron-quasi-particle random phase approximation (pn-QRPA) model was employed for the investigation of the deformation on the computed ECC [6] and EC rates in stellar matter for the *fp*-shell nuclei [7]. These EC rates were found larger than the past computations when compared at high stellar temperatures.

Recently, pn-QRPA and IBM-1 have been used for the investigation of some nuclear properties for some nuclei as

* *Corresponding author.*
E-mail address: asimullah844@gmail.com
ORCID: 0000-0002-2653-310X (Asım.ullah), 0000-0003-4521-4259 (Muhammed.riaz), 0000-0002-8229-8757 (Jameel-un.nabi), 0000-0002-8065-9993 (Mahmut.böyükata), 0000-0001-5989-6663 (Necla.çakmak)

reported in Refs. [8-10]. In the current paper, the pn-QRPA model with deformed basis is utilized to calculate the GT strength and ECC on even-even ^{46,48,50}Cr isotopes. Furthermore, the impact of the deformation parameter (β) on the calculated GT strength and ECC for the selected cases is explored. The next section describes the essential theoretical framework used in our calculation. We display our results in Section-III. Conclusions are stated in Section-IV.

2. Model Description

The pn-QRPA model was used to calculate the GT (charge-changing) strength distribution and associated ECC on the selected chromium isotopes in the stellar matter. The following Hamiltonian was considered

$$H^{QRPA} = H^{sp} + V^{ph}_{GT} + V^{pp}_{GT} + V^{pair} , \qquad (1)$$

where H^{sp} is the single particle Hamiltonian, V^{ph}_{GT} and V^{pp}_{GT} are the particle-hole GT force and particle-particle GT force respectively. The last term V^{pair} stands for the pairing force for which the BSC approximation was considered. The wave functions and single particle energies were computed within the formalism of Nilsson model [11], in which the β value was incorporated. The particle-particle and particle-hole parameter were optimized such that the experimental half-lives of the nuclei were reproduced. The Ikeda sum rule [12] was accomplished. The Nilsson potential parameters (NPP) were taken from Ref. [13] and $\hbar\omega = 41A^{1/3}$ was taken as oscillator constant for both neutrons and protons. Q-values were taken from Ref. [14] and the traditional relation $\Delta_p = \Delta_n = 12/\sqrt{A}$ (MeV) was considered for estimation of pairing gaps.

The electron capture (EC) and positron decay (PD) weak-rates from parent state "m" to daughter state "n" are given by

$$\lambda^{EC(PD)}_{mn} = \ln 2 \frac{f^{EC(PD)}_{mn}(T,\rho,E_f)}{D/B_{mn}}, \qquad (2)$$

where B_{mn} is the nuclear reduced transition probability and is given by

$$B_{mn} = B(F)_{mn} + (g_A/g_V)^2 B(GT)_{mn} , \qquad (3)$$

The values of D and g_A/g_V were taken as 6143s [15] and -1.254 [16], respectively.

The reduced Fermi ($B(F)_{mn}$) and GT ($B(GT)_{mn}$) transition probabilities were calculated using the following reduced transition probabilities:

$$B(F)_{mn} = \frac{1}{2J_m+1} \left| \langle n|| \sum_k t^k_+ ||m\rangle \right|^2, \qquad (4)$$

$$B(GT)_{mn} = \frac{1}{2J_m+1} \left| \langle n|| \sum_k t^k_+ \sigma^{\to k} ||m\rangle \right|^2, \qquad (5)$$

here J_m shows the total spin of the parent state $|m\rangle$, $\sigma^{\to k}$ is the Pauli spin matrix and t^k_+ refer to the iso-spin raising operator.

The computation of ECC is governed by the weak-interaction Hamiltonian, given by

$$\widehat{H}_\omega = \frac{G_F\cos\theta_c}{\sqrt{2}} j^{lept}_\mu \hat{J}^\mu \qquad (6)$$

The terms θ_c and G_F in the above equation, stands for Cabibbo angle and Fermi coupling constant, respectively. The $\hat{J}^\mu$ and j^{lept}_μ are the hadronic and leptonic currents, respectively, given by

$$j^{lept}_\mu = \overline{\psi}_{\upsilon_e}(x)\gamma_\mu(1 - \gamma_5)\psi_{\upsilon_e}(x) \qquad (7)$$

$$\hat{J}^\mu = \overline{\psi}_p(x)\gamma_\mu(1 - C_A\gamma_5)\psi_n(x) \qquad (8)$$

where $\psi_{\upsilon_e}(x)$ show the spinor operator. The terms γ_μ and γ_5 are stands for Dirac γ-matrices. C_A is a constant which comes as a consequence of the internal structure of the hadrons. Our main goal was to compute the ECC which is based on nuclear matrix elements from parent state $|m\rangle$ to daughter state $|n\rangle$ and is described by;

$$\langle n||\widehat{H}_\omega||m\rangle = \frac{G}{\sqrt{2}} l^\mu \int d^3x e^{-iq.x}\langle n|\hat{J}_\mu|m\rangle \qquad (9)$$

The term q in the equation refers to the three-momentum transfer and $l^\mu e^{-iq.x}$ stands for the leptonic matrix element which was employed in matrix elements calculation [17,18]. We applied the low momentum transfer approximation $q \to 0$ in this work. Such approximation enables the GT operator $(GT^+ = \sum_i \tau^+_i \sigma_i)$ to contribute dominantly to the total ECC [18]. The total ECC in the stellar condition in terms of incident electron energy (E_e) may then be computed using the following equation

$$\sigma(E_e,T) = \frac{G^2_F\cos^2\theta_c}{2\pi} \sum_m F(Z,E_e) \frac{(2J_m+1)\exp\left(\frac{-E_m}{kT}\right)}{G(A,Z,T)}$$

$$\times \sum_{J,f}(E_e - Q + E_m - E_m)^2 \frac{|\langle m|GT^+|n\rangle|^2}{(2J_m+1)} \qquad (10)$$

The Fermi function denoted by $F(Z,E_e)$ in the above equation was calculated using the recipe of Ref. [19]. To compute the famous nuclear partition function $G(Z,A,T)$, we used the prescription recently introduced in Refs. [20,21]. This recipe is believed to give a more realistic estimate of the partition functions appearing in Eq. (10). The final term in Eq. (10) corresponds to the nuclear matrix elements of $(GT^+ = \sum_i \tau^+_i \sigma_i)$ operator between final and initial states.

The underlying theme of this current work was to study the influence of the β parameter on the calculated GT strength distribution and ECC for the given Cr isotopes. To accomplish the objective, three different β values listed in Table 1 were considered. Two of β values were calculated employing theoretical models: Macroscopic-microscopic (mac-mic) model [22] and IBM-1 [23].

The Mac-mic model computed the electric quadrupole moment (Q_2). We used the value of Q_2 in the following equation to determine the deformation parameter:

$$\beta = \frac{125 Q_2}{1.44 A^{2/3}Z} \qquad (11)$$

For the calculation of deformation parameters within the IBM-1 model; first the energy levels of the given nucleus were calculated with a simplified model Hamiltonian by fitting its parameters taken as constants;

$$\hat{H} = \epsilon\hat{n}_d + \kappa \hat{Q} \cdot \hat{Q} + \kappa'\hat{L} \cdot \hat{L} , \qquad (12)$$

where $\hat{n}_d$ and $\hat{L}$ are the boson-number and the angular momentum terms, respectively. Other term is the quadrupole operator given by

$$\hat{Q}_\mu = \left[d^\dagger \times \tilde{s} + s^\dagger \times \tilde{d}\right]^{(2)}_\mu + \chi\left[d^\dagger \times \tilde{d}\right]^{(2)}_\mu, \qquad (13)$$

where χ is the fourth parameter and four parameters in total were fitted for given Cr isotopes. Later, the potential energy surfaces of the given nucleus was plotted as function of deformation parameters to calculate the β value. The potential energy surface can be formulated [24-28] from the given model Hamiltonian Eq. (12) as following;

$$V(\beta,\gamma) = N\frac{\beta^2}{1+\beta^2}\left[\epsilon + \kappa'6 + \kappa\left(\frac{5+(1+\chi^2)\beta^2}{\beta^2},\right.\right.$$

$$\left.\left. +\frac{N-1}{N}\frac{\frac{2\chi^2\beta^2}{7}-4\sqrt{\frac{2}{7}}\chi\beta cos(3\gamma)+4}{1+\beta^2}\right)\right], \qquad (14)$$

where it is seen that the $\epsilon, \kappa, \kappa'$, and χ parameters are the common constants given in Eqs. (12-13), N is the boson number of the nucleus and the β, γ are called as deformation parameters having same role Bohr-Mottelson model [29].

The experimental β values were computed by employing the following equation

$$\beta = \frac{4\pi}{3ZR_0^2} \times \left[\frac{B(E2)\uparrow}{e^2}\right]^{1/2} \qquad (15)$$

where $R_0^2 = 0.0144\,A^{2/3}b$ and $B(E2)\uparrow$ is in units of e^2b^2. The reduced electric quadrupole transition probability $B(E2)\uparrow$ was taken directly from the National Nuclear Data Center (NNDC) [30].

3. Results and Discussions

In Table 1, fitted parameters of the simplified Hamiltonian given in Eq. (12) are listed and these parameters are also taken as the constant in the energy surface formalism. The units of ϵ, κ, and κ' parameters are in keV and χ is dimensionless.

Table 1. The fitted parameters (keV) given as constant in Eqs. (12-13) and χ is dimensionless.

Isotopes	ϵ	κ	κ'	χ
^{46}Cr	0.8742	- 0.0485	-	-0.45
^{48}Cr	1.5155	- 0.2333	- 0.0687	-1.02
^{50}Cr	1.2002	- 0.1565	- 0.0386	-0.5

The energy spectra including the calculated and experimental energy levels of the given isotopes are plotted in Figure 1. The calculated levels are marked by the black solid line and the experimental ones [30] given with the blue dashed lines. As seen from this figure the calculated energy levels with IBM-1 are quite close to the experimental ones [30].
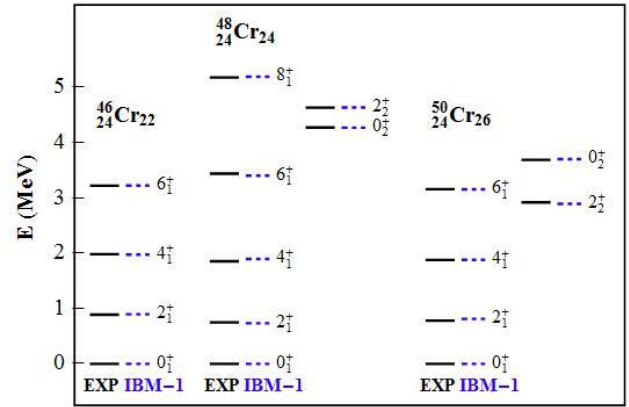

Figure 1. The experimental [29] and the calculated energy levels of selected Cr isotopes.

In Figure 2, the potential energy surfaces of IBM-1 are plotted in terms of β parameter ($\gamma=0$) for given Cr isotopes. The β parameters of each isotope can be calculated from the minimum point of the energy surfaces. These values are listed in Table 2. As seen from Figure 2, ^{46}Cr has a spherical shape since this parameter is zero whereas ^{48}Cr and ^{50}Cr have deformed prolate shape. The even-even ^{46}Cr, ^{48}Cr, and ^{50}Cr isotopes display shape changing from spherical to prolate along the isotopic chain for $22 \leq N \leq 26$.
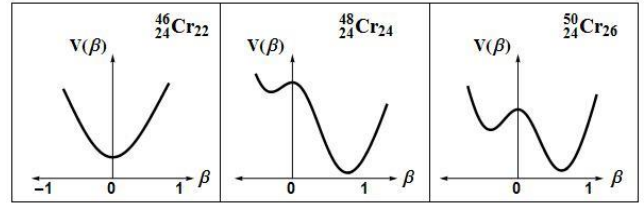

Figure 2. The energy surfaces as function of β parameter for the given Cr isotopes.

Table 2 summarizes the centroid and total GT strength values, computed from the calculated GT strength distributions for the selected Cr isotopes. The third column shows the values of β parameter computed employing the respective models given in second column of Table 2. The previous section described how these values were calculated. The table reflects that the total GT strength lowers as the mass number increases. This outcome can be attributed to the fact that the EC process turns more difficult for higher neutron number. The centroid value decreases for heavier cases because the neutron excess increases. The table also shows the effect of deformation on the computed GT strength. It is noted that for each isotope, with increase in the value of β the calculated GT strength decreases. This is an interesting outcome, but we cannot generalize this statement which requires further investigation currently in progress.

Table 2. The computed centroid and total GT strength values for the obtained β_2 parameter for the given Cr isotopes.

İsotopes	Model	Deformation Parameter β	Total GT strength $\sum B(GT_+)$	Centroid $\overline{E}_+$ (MeV)
^{46}Cr	Mac-mic	0.028	9.13	12.37
	IBM-1	0	9.67	12.15
	NNDC	0.288	8.97	12.76
^{48}Cr	Mac-mic	0.23551	8.94	11.74
	IBM-1	0.760	8.46	12.02
	NNDC	0.368	8.63	11.95
^{50}Cr	Mac-mic	0.14124	8.58	10.78
	IBM-1	0.586	5.75	11.14
	NNDC	0.29	7.66	10.94

Figure 3 displays the computed ECC on ^{46,48,50}Cr as a function of incident electron energy (E_e) in the range (0–30) MeV. It is found that for each Cr isotope the ECC increases with increasing incident electron energy (E_e) because of the term $(E_e - Q + E_m - E_m)^2$ in Eq. (10). It is also noted the ECC increases exponentially in the energy range (1–1.5) MeV. When the temperature of the core rises from 0.5 MeV to 1.0 MeV, there is a prominent increase in the calculated ECC value up to a factor 50. Configuration mixing and thermal unblocking of states could be cited as probable sources for this increment [31]. With a further increase in temperature from 1.0 MeV to 1.5 MeV, the increment in the computed ECC is very small (less than a factor of 2). This is because majority of the transitions are already unblocked at such high temperatures. The steep increase may be attributed to the behavior of the computed GT strength distribution. The centroid of the GT strength distribution shifts by few MeV with rise in temperature. The nuclear partition functions also increase with rise in core temperature. These factors are responsible for the change in behavior of the ECC.
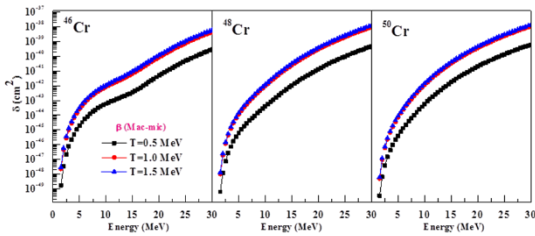

Figure 3. Calculated ECC on ^{46,48,50}Cr as a function of incident electron energy for different values of temperature at β parameter (Mac-mic).

Lastly we investigated the impact of the β parameter on computed ECC for the given isotopes. Figure 4 shows the calculated ECC as a function of the β parameter at a fixed temperature of 1 MeV. It can be noted from the figure that the computed ECC on the selected Cr isotopes decreases with decrease in β value and vice versa.
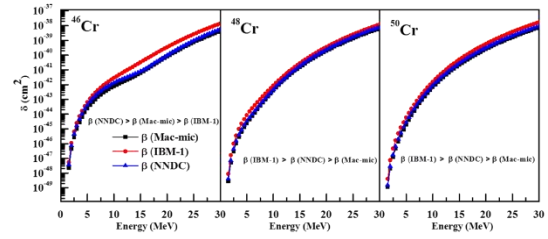

Figure 4. Comparison of the computed ECC on ^{46,48,50}Cr with different β values, at fixed temperature (T = 1 MeV).

4. Summary

The fundamental theme of the presented study was to explore the influence of the β parameter on the calculated GT strength distributions and ECC. To accomplish the goal, we considered three even-even Cr isotopes and calculated the ECC for these cases at three different temperatures (0.5, 1 & 1.5 MeV). The GT strength distributions obeyed the ISR and were widely dispersed among all the daughter states of the respective nuclei. The centroid and total GT strength values were computed in terms of the β parameter. It was found that the total GT strength has inverse relation with the β parameter i.e with decreasing β, the total GT strength increases and vice versa. The computed ECC for the given cases was noted increasing with increase in the core temperature. Comparing the computed ECC at different β values, it was found that they increased with rise in the value of β parameter. Moreover, the selected ^{46}Cr, ^{48}Cr, and ^{50}Cr isotopes exhibit shape changing from spherical to prolate. We are studying more isotopes of chromium and hope to report soon on our findings.

References

[1] G. M. Fuller, W. A. Fowler and M. J. Newman, Astrophys. J. Suppl. Ser. 42 (1980).

[2] E. M. Burbidge, G. R. Burbidge, W. A. Fowler and F. Hoyle, Rev. Mod. Phys. 29 (1957) 547.

[3] P. G. Giannaka and T. S. Kosmas, Electron Capture Cross Sections for Stellar Nucleosynthesis, Adv. H. E. Phys. 2015, (2014) 11.

[4] G. Martìnez-Pinedo, K. Langanke, D. J. Dean, Astrophys. J. Suppl. Ser. 126 (2000) 493.

[5] A. Heger, K. Langanke, G. Martìnez-Pinedo, S. E. Woosley, Phys. Rev. Lett. 86 (2001) 1678.

[6] A. Ullah, J.-U. Nabi and M. Riaz, Int. J. Mod. Phys. D 28 (2019) 2040011.

[7] J.-U. Nabi and M. Riaz, J. Phys. G: Nucl. Part. Phys. 47, (2019) 085201.

[8] J.-U. Nabi, M. Böyükata, Nucl. Phy. A 947 (2016) 182.

[9] J.-U. Nabi, Böyükata, Astrophys Space Sci. 362 (2017) 9.

[10] J.-U. Nabi, M. Ishfaq, M. Böyükata, M. Riaz, Nucl. Phy. A 966 (2017) 1.

[11] S. G. Nilsson, G Nilsson, Mat. Fys. Medd. K. Dan. Vidensk. Selsk. 29 (1955) 16.

[12] K. Ikeda, S. Fujii and J. I. Fujita, Phys. Lett. 3, (1963) 271.

[13] I. Ragnarsson and R. K. Sheline, Phys. Scr. 29, (1984) 385.

[14] G. Audi, F. Kondev, M. Wang, W. Huang, and S. Naimi, Chinese physics C, 41 (2017) 030001.

[15] K. Nakamura, (Particle Data Group): J. Phys. G, Nucl. Part. Phys. 37, (2010) 075021.

[16] J. C. Hardy, and I. S. Towner, Phys. Rev. C 79, (2009) 055502.

[17] N. Paar, G. Col'o, E. Khan, and D. Vretenar, Phys. Rev.C 80 (2009) 055801.

[18] J. D. Walecka, Theoretical nuclear and subnuclear physics, (World Scientific Publishing Company, 2004).

[19] N. Gove and M. Martin, At. Data Nucl. Data Tables, 10 (1971) 205-219.

[20] J.-U. Nabi, A. N. Tawfik, N. Ezzelarab, and A. A. Khan, Astrophys. and Space Sc. 361 (2016) 71.

[21] J.-U. Nabi, A. N. Tawfik, N. Ezzelarab, and A. A. Khan, Phys. Scr. 91 (2016) 055301.

[22] P. Moller and J. R. Nix, At. Data Nucl. Data Tables, 26 (1981) 165-196.

[23] A. Arima and F. Iachello., Annals of Physics 99 (1976) 253-317.

[24] A. E. L. Dieperink, O. Scholten and F. Iachello, Phys. Rev. Lett. 44 (1980) 1747.

[25] A. E. L. Dieperink, O. Scholten, Nucl. Phys. A 346 (1980) 125.

[26] J. N. Ginocchio, M. W. Kirson, Phys. Rev. Lett. 44 (1980) 1744.

[27] J. N. Ginocchio, M. W. Kirson, Nucl. Phys. A 350 (1980) 31.

[28] P. Van Isacker and J.-Q. Chen, Phys. Rev. C 24 (1981) 684.

[29] A. Bohr and B. R. Mottelson, Nuclear Structure. Volume 2: Nuclear Deformation, World Scientific Publishing, 1998.

[30] National Nuclear Data Center (NNDC), http://www.nndc. bnl.gov/, 2019.

[31] K. Langanke, E. Kolbe, and D. Dean, Phys. Rev. C, 63 (2001) 032801.

The effects of changing story number and structural footprint area on building performance in reinforced-concrete buildings

Ercan Işık[a] (ID), Nursima Sayın[b] (ID), Ali Emre Ulu[a],* (ID)

[a]Bitlis Eren University, Department of Civil Engineering, TR-13000, Bitlis Turkey
[b]Bitlis Eren University, Graduate Education Institute, TR-13000, Bitlis Turkey

ARTICLE INFO

ABSTRACT

Structural footprint area and number of stories occupy an important place among the factors affecting the behavior of buildings under earthquake effects. In this study, footprint area and number of stories are considered as two different variables. A sample reinforced-concrete building with all values such as structural system elements, dimensions, materials, material models and loading status is selected same in all different structural models. The structural analyzes were made for a single direction since the structure was chosen symmetrically. In each building model, the axle clearance has been increased by one meter in both directions. As the second variable, four different story numbers were chosen as 5, 6, 7 and 8. Eigenvalue and static pushover analyzes were performed for the each structural model. Target displacement for damage estimation, period, stiffness and base shear force values were obtained for all models, respectively. Both, Eurocode 8-Part 3 and Turkish Seismic Design Code-2018 were considered in the analysis. As the building footprint area and number of story increase, period, displacement and target displacement increase for both codes.

1. Introduction

There are many parameters that can adversely affect the behavior of structures under loads. Determining the behavior of the structures under loads is directly related to their structural characteristics. The number of total stories is the one of important factor that determines the degree of damage in reinforced-concrete (RC) buildings after devastating earthquakes. There is a direct relationship between the number of stories and earthquake damages (Şengezer, 1999; Sucuoğlu, 2007; Yakut, 2004; Işık, 2016; Hadzima-Nyarko and Šipoš, 2017; Özdemir et al., 2016; Işık et al., 2018). A great number of design variables were affect to the construction costs and structural analysis besides number of stories. These variables can be specified as shape and complexity of buildings plan, height of stories and service requirements of the building (İlerisoy and Tuna, 2018; Saidu et al., 2015).

It is important to give the necessary dimensions to the structural characteristics. The structural and non-structural system elements and other structural features that require size were expressed in three dimensions. The structural footprint area of the building keeps out an important role in the concept of size (Işık and Karaşin, 2020). The dimension of footprint area was calculated by width and length of the building. These dimensions were obtained from the sum of the axle openings forming the structural system.

Within the scope of this study, both the number of stories and structural footprint area were selected as variable for a sample RC building. Four different number of story was chosen as 5, 6, 7 and 8 in this study. The second variable was selected as footprint area. The selections were made changing the axle openings in both directions. Each axle clearance was selected as 4m, 5m and 6m in both X and Y direction. The structural footprint area of the sample RC building model was changed according to axle clearance. Eigen value and static pushover analysis were performed for

all structural models that considered in this study. Target displacement for damage estimation, period, frequency, stiffness and base shear force values were obtained for all models through these analysis, respectively.

In the study, firstly, information was given about the types of analysis used. In the next section, detailed information about the structural models used in the study is expressed. In the next section, detailed information about the structural models used in the study is expressed. The results were interpreted and suggestions were made.

Most of the structures in Turkey are constructed with RC system. This study focuses on the interaction of horizontal and vertical dimensions with each other especially in RC structures under earthquake effects. Earthquake damages in RC structures reveal the importance of these two parameters. In this respect, this study can contribute in terms of science and practice for RC buildings.

2. Method

Eigenvalue and static pushover analysis were used in this study for structural analysis. Eigen value analyzes were conducted primarily for the building models created for each variable used in this study. Mode shapes and natural frequency for any structure can be obtained by eigenvalue analysis. Material properties always remain constant during the calculation. Briefly, it can be evaluated as pure elastic structural analysis. Structure-related modal period, frequency, modal participation factors, effective modal masses and their percentile values can be reached by eigen value analysis (Antoniou and Pinho, 2003; Seismossoft, 2014; Kutanis et al., 2017; Nikoo et al., 2017).

Static pushover analysis was used another analysis that used in this study. Earthquake performance and damage conditions of buildings can be calculated with this analysis generally. Static pushover analysis is called as non-linear calculation method, which is made by increasing the horizontal loads gradually under fixed vertical loads in RC structures. The earthquake impact analysis and accurate results for behaviour of building can be performed with this analysis more realistically. Deformation behaviours of all elements of the building and the inelastic behaviour of the material can be examined with this method (Estêvão and Oliveria, 2015; Ademovic et al., 2013; Chopra and Goel, 2002; Işık and Kutanis, 2015; Işık and Özdemir, 2017). A typical static pushover curve is shown in Figure 1.
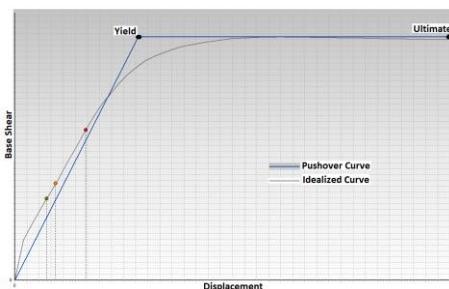

Figure 1. A typical static pushover curve

2.1. Structural characteristics of building models

Within the scope of the study, a sample RC building with different story numbers and structural footprint area was chosen. The structure was chosen symmetrically in both X and Y directions. The blueprint of the sample building was shown in Figure 2.
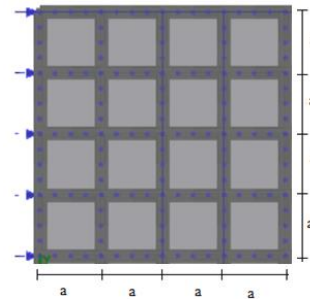
Figure 2. The blueprint of sample RC building

Analyzes were carried out under the Seismostruct software under an academic license (Seismosoft, 2016). The soil class was selected as ZE for all structural models. The building importance class was taken into account as the II. Class, thedampingratio as 5% and peak ground acceleration was selected 0.240g. Number of stories was kept constant and a value for footprint was selected as variable. For the value for a three different cases were considered. Considered structural dimensions are given in Table 1.

Table 1. Dimensions of the building models considered

Model No	a (m)	a (m)	Footprint Area (m²)
Model 1	4.0	4.0	256
Model 2	5.0	5.0	400
Model 3	6.0	6.0	576

2D model of the buildings and loads applied to the models were shown in Figure 3.
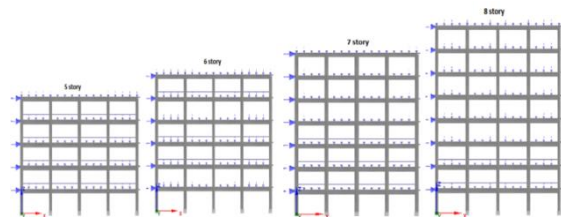
Figure 3. 2D building models for different number of stories

3D structural models that obtained from software were given in Figure 4.

Figure 4. 3D building models for different number of stories

C25-S420 was taken into consideration for RC structure. The transverse reinforcements were selected as φ10/10 in columns and φ10/15 in beams. The reinforcements used in all columns were selected as 4φ20 in corners, 4φ16 in top-bottom sides and 4φ16 in left-right sides. The reinforcements u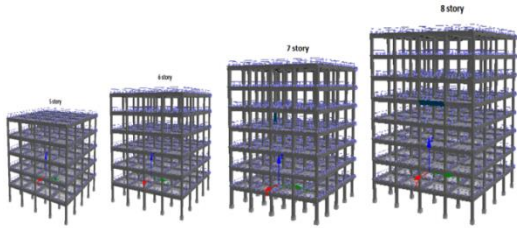sed in all beams were selected as 4φ16 in lower, 5φ18 in upper, 2φ12 in sides, 4φ10 in lower-slab and 6φ10 in upper-slab. Column and beam cross sections used in the reinforced concrete building are given in Figure 5.
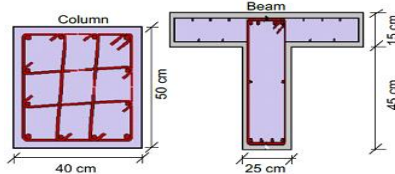

Figure 5. Beam and columns cross-sections

All these structural characteristics were instant in all structural models that used in this study. The variables were total number of stories and footprint area.

2.2. Analysis Results

Base shear force, elastic stiffness (K_elas) and effective stiffness (K_eff) were calculated separately for each number of stories and each structural model. The displacement values for damage estimation for structural models were obtained for three damage status according to Eurocode-8, Part 3 firstly. These are near collapse (NC), significant damage (SD) and damage limitation (DL). All these results were given in Table 2.

Table 2. Analysis results for all structural models

Model	Period (s)	Base Shear (kN)	K_elas	K-eff	DL	SD	NC
5 story							
1	0,3494	6111,5	195509	90309	0.027	0.034	0.059
2	0.3933	6321.05	180846	85362	0.030	0.038	0.066
3	0.4368	6505.9	167281	80496	0.033	0.042	0.074
6story							
1	0.4191	6274.1	168927	77966	0.031	0.040	0.070
2	0.4712	6515.5	157325	73661	0.035	0.045	0.078
3	0.5230	6722.9	151360	69585	0.039	0.050	0.087
7story							
1	0.4898	6421.5	147297	68383	0.036	0.047	0.081
2	0.5497	6687.2	144829	65088	0.040	0.052	0.090
3	0.6097	6914.7	141399	60879	0.045	0.058	0.100
8story							
1	0.5615	6528.4	141882	61010	0.041	0.053	0.091
2	0.6290	6830.7	133670	58052	0.046	0.059	0.102
3	0.6971	7075.9	124809	54417	0.051	0.065	0.113

The first value refers to displacement at the moment of yield (d_y), the second value refers to the intermediate (d_{int}) displacement and the third value refers to the target displacement (d_t). All these displacement values were obtained from pushover curves and shown in Table 3.

Table 3. Comparison of the displacements

Model	d_y(m)	d_{int} (m)	d_t(m)
5 story			
1	0.0677	0.1260	0.300
2	0.0740	0.1320	0.300
3	0.0810	0.1440	0.300
6 story			
1	0.0805	0.1380	0.300
2	0.0885	0.1500	0.300
3	0.0966	0.1620	0.300
7 story			
1	0.0939	0.1560	0.300
2	0.1027	0.1680	0.300
3	0.1136	0.1860	0.300
8 story			
1	0.1070	0.1800	0.300
2	0.1177	0.1920	0.300
3	0.1300	0.2040	0.300

The comparison of pushover curves that obtained from structural analysis for different structural footprint area for 5-story was given in Figure 6; 6-story was given in Figure 7;7-story was given in Figure 8 and 8-story was given in Figure 9.
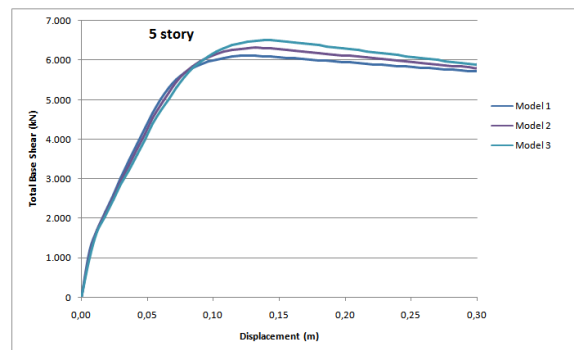

Figure 6. The comparison of pushover curves for 5-story for different structural models
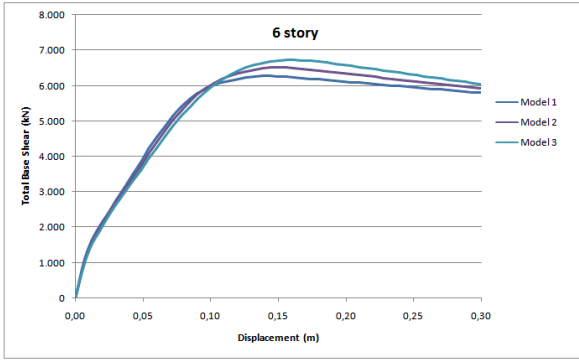
Figure 7. The comparison of pushover curves for 6-story for different structural models

Figure 8. The comparison of pushover curves for 7-story for different structural models

Figure 9. The comparison of pushover curves for 8-story for different structural models
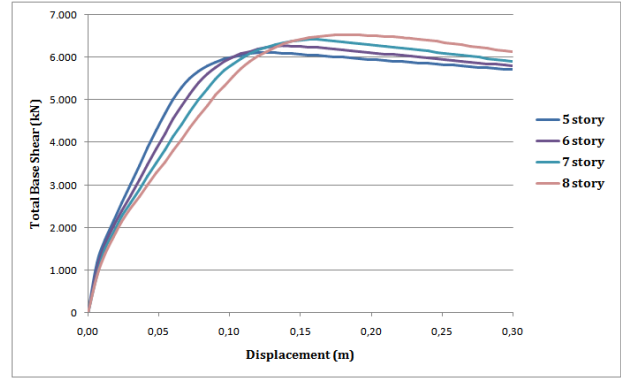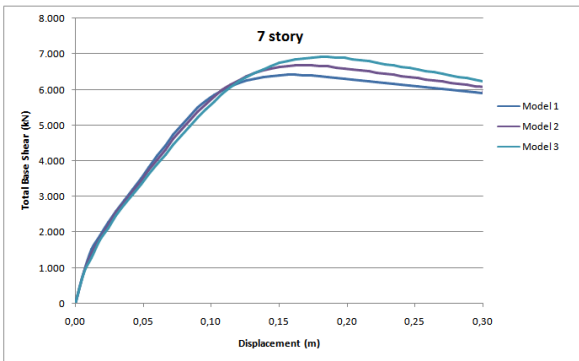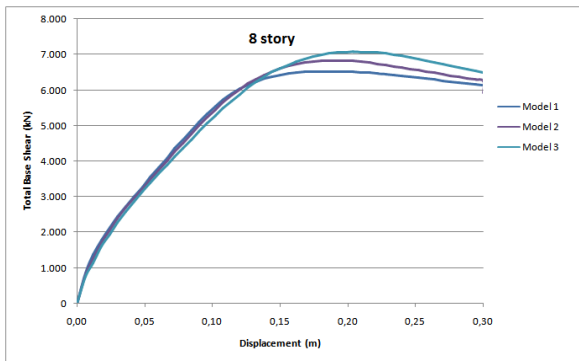
The comparison of pushover curves for different number of stories for Model 1 was given in Figure 10. The pushover curves for other structural models were obtained same. So only for Model 1 was given.

Figure 10. The comparison of pushover curves for different story number for Model 1

The period and displacement values for damage estimation for structural models were obtained for three damage status according to Turkish Seismic Design Code -2018 (TSDC-2018). These values were given in Table 4.

Table 4. The results according to TSDC-2018

Model	Period (s)	Continuous Use (KK)	Immediate Occupancy (HK)	Life Safety (CG)	Collapse Prevantation (BP)
5 story					
1	0.593294	0.02078	0.02909602	0.039487	0.04780
2	0.658507	0.02315	0.03241832	0.043996	0.053258
3	0.72239	0.02550	0.03570315	0.048454	0.058655
6 story					
1	0.71297	0.02507	0.03510615	0.047644	0.057674
2	0.790192	0.02789	0.03905054	0.052997	0.064154
3	0.866262	0.03069	0.04297596	0.058324	0.070603
7 story					
1	0.834032	0.02942	0.04119793	0.055911	0.067682
2	0.922894	0.03267	0.04574184	0.062078	0.075147
3	1.010913	0.03592	0.05029363	0.068255	0.082625
8 story					
1	0.956597	0.03384	0.04737902	0.06430	0.077836
2	1.056697	0.03749	0.05249742	0.071246	0.086245
3	1.156408	0.04118	0.05765996	0.07825	0.094727

3. Results

The importance of structural dimensions and number of stories were mentioned within the scope of the study. Structural dimensions and total number of stories in the building can take different values due to different reasons. Within the scope of this study, two different structural analyses were carried out considering the change in the number of stories and structural dimensions. It is determined that there is a complete agreement between all the results obtained.

As the structural footprint area increased, the structure became less rigid. Consequently, the period value decreased as the footprint area decreased and seismic capacity decreased in RC structures. As the number of story decreases, the period value increases, the stiffness value decrease and seismic capacity increase. The increase in the footprint area and number of story caused the structure to be less rigid.

As a result of the analyses, the greatest percentages of change were observed at the target displacements predicted for the structure. Target displacement values for the settlement at the moment of yield (dy), near collapse (NC), significant damage (SD) and damage limitation (DL) increased depending on the footprints and number of stories. The increase in target displacements in terms of performance criteria reveals the direct relationship between the damage occurring in the earthquake and the number of stories in RC structures.

The period and displacements for damage estimation were calculated for Eurocode 8, Part 3 and TSDC-2018, respectively in this study. A complete agreement has been achieved between these values obtained for Eurocode 8 and TSDC- 2018, separately according to changing structural footprint area and number of stories. However, the period values obtained for TSDC-2018 were higher than Eurocode-8. Period values increase because of TSDC -2018 allows more translation of structures.

According to TSDC - 2018, both elastic and effective stiffness values decreased as the number of floors increased. As a result, period values also increased. Period values increased as the building structural footprint area increased. Target displacement values calculated for performance levels depending on TSDC-2018 increased as the number of stories increased. These target displacements increased as the structural footprint area increased. As the number of stories and structural footprint area increases, expected performance levels are a result of the need to increase.

The importance of structural dimensions and number of floors were mentioned within the scope of the study. Unnecessary increase in dimensions and number of floors adversely affects structural analysis.

References

Ademovic, N., Hrasnica, M., Oliveira, D.V., 2013. Pushover analysis and failure pattern of a typical masonry residential building in Bosnia and Herzegovina. Engineering Structures, 50, 13-29.

Antoniou, S., Pinho, R., 2003. Seismostruct – Seismic Analysis program by Seismosoft. Technical manual and user manual.

Chopra, A.K., Goel, R.K., 2002. A modal pushover analysis procedure for estimating seismic demands for buildings. Earthquake Engineering & Structural Dynamics, 31(3), 561-582.

Estêvão, J. M., Oliveira, C. S., 2015. A new analysis method for structural failure evaluation. Engineering Failure Analysis, 56, 573-584.

Hadzima-Nyarko, M., KalmanSipos, T., 2017. Insights from existing earthquake loss assessment research in Croatia. Earthquakes and Structures, 13(4), 365-375.

İlerisoy, Z.Y., Tuna, M.E. 2018. Effects of plane dimensions and number of storeys on the cost of rectangular-plane buildings constructed with tunnel Form Megaron, 13(4), 559-568.

Işık, E., 2016. Consistency of the rapid assessment method for reinforced concrete buildings. Earthquakes and Structures, 11(5), 873-885.

Işık, E., Karaşin, İB., 2020, The mutual interaction between the structural footprint and number of floors in steel structures . Unpublished article.

Işık, E., Kutanis M., 2015. Performance based assessment for existing residential buildings in Lake Van basin and seismicity of the region. Earthquakes and Structures, 9(4), 893-910.

Işık, E., Özdemir, M., 2017. Performance based assessment of steel frame structures by different material models. International Journal of Steel Structures, 17(3), 1021-1031.

Işık, E., Özdemir, M., Karaşin, İ. B., 2018. Performance analysis of steel structures with A3 irregularities. International Journal of Steel Structures, 18(3), 1083-1094.

Işık, E., Işık, M. F., & Bülbül, M. A. 2017. Web based evaluation of earthquake damages for reinforced concrete buildings. Earthquakes and Structures, 13(4), 387-396.

Kutanis, M., Boru, E. O., Işık, E., 2017. Alternative instrumentation schemes for the structural identification of the reinforced concrete field test structure by ambient vibration measurements. KSCE Journal of Civil Engineering, 21(5), 1793-1801.

Özdemir, M., Işık, E., Ülker, M., 2016. Performance evaluation of reinforced concrete buildings with different story numbers. BEU Journal of Science, 5(2), 183-190.

Pinto, P. E. (2005). The Eurocode 8-Part 3: the new European Code for the seismic assessment of existing structures.

Saidu, İ.,Alumbugu, P.O., Abdulazeez, A., Ola-Awo, W.A., 2015. Assessment of the effect of plan shapes on cost of institutional buildings in Nigeria, International Refereed Journal of Engineering and Science (IRJES), 4(3), 39-50.

SeismoStruct, 2016. A computer program for static and dynamic nonlinear analysis of framed structures. Seismosoft.

Şengezer, B.S.1999. The damage distribution during March 13, 1992 Erzincan earthquake. YT U. Press Release Center, 13.

Sucuoğlu, H., 2007. A screening procedure for seismic risk assessment in urban building stocks. Sixth National Conference on Earthquake Engineering, Istanbul, Turkey.

Turkey Seismic Design Code (TSDC-2018), Ankara, Turkey.

Yakut, A., 2004. Preliminary seismic performance assessment procedure for existing RC buildings. Engineering Structures, 26(10), 1447-1461.

Radon concentration measurements in surface water samples from Van Lake, Turkey using CR-39 detectors

Halime Kayakökü[a],* , Mahmut Doğru[b]

[a] Bitlis Eren University, Department of Physics, TR-13000, Bitlis Turkey

[b] Fırat University, Department of Physics, TR-23169, Elazığ Turkey

ARTICLE INFO

ABSTRACT

In this study, radon concentration was examined in surface water samples taken from Van Lake in spring and autumn. The samples were taken along the coastline from Tatvan, where the active fault line lies, until Erciş. Analyses were performed by using CR-39 solid nuclear track detectors and RadoSYS radon measurement system. Radon measurement parameters (C_{Rn}, E_s, E_m and EC_{Ra}) were calculated with the data obtained. The results of this study were compared with the limit values given for radon in water and the results obtained in similar studies.

1. Introduction

Radon is a noble gas with a half-life of 3.82 days and it occurs as a result of the radioactive conversion of ^{226}Ra (Radium) located in the decay chain of ^{238}U (Uranium). Radioactive radon gas, which is colorless, odorless, tasteless and short-lived decay products in the atmosphere account for about 50 % of the radiation that people are exposed to from natural sources (UNSCEAR, 2000). ^{222}Rn, which is approximately seven times heavier than air, is collected in hollows and dissolved in water (Alkan and Göksel, 1975). It is not possible to find water in its pure form in the natural environment. Radiation pollutes water and threatens human health. The contamination of water by radiation results from the natural radioisotopes in the atmosphere and soil, reactor accidents, nuclear weapon tests and medical radioactive wastes (Yaramış, 1985). Besides the solubility of radon gas in water there is also a tendency to escape into the environment where the dissolved radon is located. As a result, high radon concentrations in groundwater and thermal waters, it poses a

great danger not only for people who drink water, but also for people who breathe it (UNSCEAR, 2000).

One of the significant factors that need to be determined in terms of water usability is the level of radioactivity. For this reason, the conformity of drinking and domestic water to standards should be investigated with analyses on the radioisotopes available in water (Varol, 2011). The natural radioactivity of the water arises from the radioactive masses or minerals, which they pass through or are in contact with.
Radon concentration in water changes depending on some factors such as the emission of radon from the rocks that the water contacts, temperature, pressure, precipitation and seismic activities (Ilani et al., 2006; Sannappa et al., 2006). Some rock types contain uranium in concentrations higher than 5 ppm. These are granites, syenites, pegmatites, acid volcanic rocks and gneisses (Shashikumar et al., 2009; UNSCEAR, 2000).
Radon measurement techniques divide into two groups as active and passive measurement techniques. In this study, the

* *Corresponding author.*
  Tel.: +90 434 222 0000; fax: +90 434 222 0101
  E-mail address: hkayakoku@beu.edu.tr
  ORCID : 0000-0003-4036-4012 *(Halime KAYAKÖKÜ)*, 0000-0002-0015-0629 *(Mahmut DOĞRU)*

passive measurement technique was employed to detect radon gas concentrations in water. CR-39 solid track detectors are frequently used in passive measurement technique (Kayakökü et al., 2016; Turhan et al., 2018; Büyükuslu et al., 2018; Alali et al., 2019).

The aim of present research study was to determine the radon concentration, effective radium content, the surface and mass diffusion rates of radon in surface water samples taken from Van Lake in spring and autumn. For this purpose, CR-39 solid nuclear track detectors were used. Radon analyzes were done using RadoSYS system.

2. Material and Method

2.1. Research area

Van Lake is located in the east of Turkey and the GPS coordinates of its geographical location are 38° 38' 27″ north and 42° 48' 45″ east. It was formed as a result of the explosion of the Nemrut volcanic mountain, which is located within the borders of the province of Bitlis. Van Lake is a volcanic embankment with a surface area of 3790 km² as an enclosed lake. The water of this lake is an alkaline lake with a salinity rate of 0.19% and pH of 9.8 on average.

Water samples were collected using a Hydro bios ruttner water sampler from 24 stations within Van Lake. 15 ml of HNO_3 (nitric acid) was added to each 1 liter of sample. (Bohus-Saja et al., 1997). In this way, pH≤2 was obtained for water samples, and it was ensured that the elements in the samples would not precipitate and stick on the surface of the sample container (Bohus-Saja et al., 1997).

Figure 1. Research area and sampling points

In present study, the radon concentrations, exhalation rates and radium contents were calculated using CR-39 detectors for forty eight surface water samples. After the water samples were placed in the sample containers, they were left for a month to ensure radioactive equilibrium. CR-39 detectors were prepared in pieces of 1 cm×1 cm dimensions. After a one-month waiting period, CR-39 detectors were placed in sample containers. Likewise, after a one-month waiting period, the detectors were removed from the containers.

The cylindrical polyethylene sample containers, in which the sample and the CR-39 detector are placed, are shown in Figure 2.
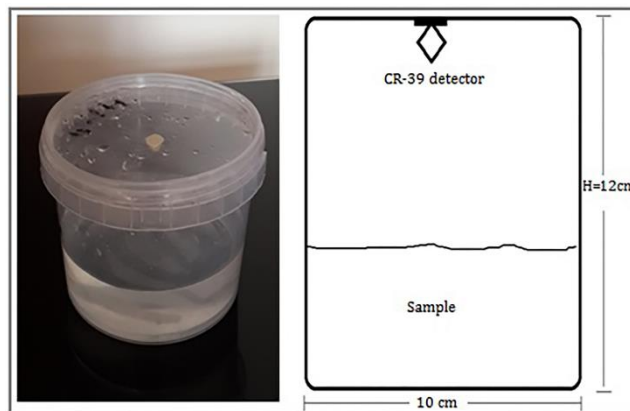

Figure 2. The structure cylindrical polyethylene sample container used for radon measurements

After the one-month waiting period was over, the sample containers were opened, and the detectors were removed from the containers. During this time, the chemical etching process was employed in order to make the traces of the alpha particles left on the detectors apparent. For this purpose, a 30% NaOH solution was prepared and distributed into the beakers equally. After the detectors were placed in the solution, the beakers were kept in the oven at 60 °C for 18 hours. Afterwards, the detectors were removed from the beakers which were taken out of the oven and then washed with pure water. Following the completion of the washing process, the detectors were kept aside for about 1 hour to dry. After drying up, the detectors were ready for the tracking procedure.

Tracks of alpha particles hitting Cr-39 detectors during the waiting period were shown in Figure 3.

Radon analysis operations were carried out using the Passive Radon Detector System (RadoSYS system) in Bitlis Eren University Nuclear Physics Research Laboratory. The radon tracking system (Figure 3) consists of a 500× magnification microscope and software connected to the computer. The program works with the LINUX operating system. First, CR-39 detectors were placed on the slides. After the detectors on the slides were divided into 144 equal parts by the optical tracking system, the traces on the detectors were counted. After the periods of keeping the detectors in the dishes containing the

samples were entered on the program, radon density and radon activity concentration were separately calculated by the program for each sample.
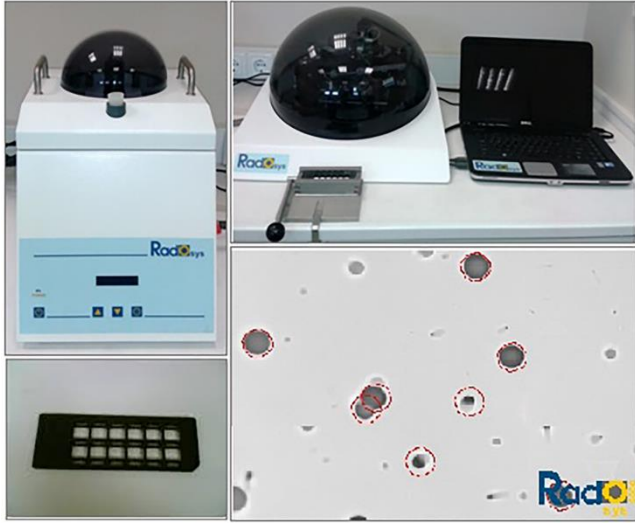

Figure 3. Radon track reading system and the tracks of alpha particles in the CR-39 detector

In Figure 3, the tracks of alpha particles hitting the CR-39 detector can be seen. While calculating radon concentrations, it is necessary to detect the background value of the detector placed in the dish when there is no sample. For this, the detectors in the sample dishes and the detector in the empty dish were tracked on the detector tracking system in the same way, and the net track densities were acquired by the subtraction of the track densities from each other.

2.2. Radon concentration calculations

After specifying the net trace densities formed on the CR-39 detectors, the radon concentrations were calculated by Equation (1) using the obtained net trace densities, the periods the detectors were kept in the sample containers and the calibration factor.

$$C_{Rn} = \frac{\rho \times f}{\Delta t} \tag{1}$$

where C_{Rn} is radon concentration (Bq/m³), ρ is net track density (track/mm²), f is calibration factor and Δt is detector exposure time (in hour) (Tokonami et al., 2005). Calibration factor for CR-39 solid nuclear trace detectors is 44.47 (kBqh/m³)/(track/mm²).

The equation used to calculate the effective radium content (EC$_{Ra}$) was shown in Equation 2.

$$EC_{Ra} = \frac{\rho \times h \times A \times f}{V \times T_{eff}} \tag{2}$$

2.3. Effective radium content (EC$_{Ra}$)

where h is distance between detector and sample (m), A is the surface area of sample container (m²), T is total exposure time (h), T_{eff} is effective exposure time [$T_{eff} = T + 1/\lambda\ (e^{\lambda T} - 1)$], V is sample volume (m³) (Jönsson et al., 1999).

2.4. Radon surface and mass exhalation rates (E$_s$, E$_m$)

Radon surface exhalation rates (E$_s$) and radon mass exhalation rates (E$_m$) were calculated using Equation (3) and Equation (4), respectively.

$$E_s = \frac{\rho \times f \times h \times \lambda}{T_{eff}} \tag{3}$$

$$E_m = E_s \times \frac{A}{M} \tag{4}$$

where, λ (2.1×10⁻⁶) is ²²²Rn decay constant, h is height of the sample container (m), A is surface area of the sample in the container (m²) and M is the mass of the sample in the sample container (kg).

3. Results and discussion

Radon concentrations (C$_{Rn}$), radon surface exhalation rates (E$_s$), radon mass exhalation rates (E$_m$) and effective radium contents (EC$_{Ra}$) for surface water samples taken in spring and autumn periods were given in Table 1 and Table 2, respectively. While the comparison of the radon concentration values in the surface water samples of the spring and autumn period with the limit value recommended by USEPA (United States Environmental Protection Agency, 2012) was shown in Figure 4 and Figure 5, respectively, the seasonal comparison of the radon concentration values was shown in Figure 6.

$$EC_{Ra} = \frac{\cdots}{V \times T_{eff}}$$

Table 1. The C_{Rn}, E_s, E_m and EC_{Ra} values of surface water sample in spring period (Kayakökü and Doğru, 2019).

Sample ID	Sample locations		C_{Rn} (Bq/m³)	E_s (Bq/m².h)×10⁻¹	E_m (Bq/m³.h)×10⁻³	EC_{Ra} (Bq/m³)
	Latitude	Longitude				
Y.S-1	38° 29' 04.3"	42° 29' 22.5"	10.00±0.92	0.12±0.01	0.14±0.01	0.08±0.01
Y.S-2	38° 30' 02.8"	42° 23' 39.8"	18.30±1.69	0.14±0.01	0.21±0.02	0.15±0.01
Y.S-3	38° 30' 03.1"	42° 18' 03.4"	43.41±4.00	0.32±0.03	1.31±0.12	0.72±0.07
Y.S-4	38° 33' 17.7"	42° 22' 11.4"	78.60±7.25	0.58±0.05	2.15±0.20	1.30±0.12
Y.S-5	38° 36' 26.5"	42° 24' 30.9"	33.85±3.12	0.25±0.02	1.02±0.09	0.56±0.05
Y.S-6	38° 39' 05.3"	42° 28' 14.7"	50.00±4.61	0.37±0.03	0.48±0.04	0.35±0.03
Y.S-7	38° 42' 56.9"	42° 26' 29.8"	31.07±2.8	0.23±0.02	0.94±0.09	0.51±0.05
Y.S-8	38° 44' 55.7"	42° 32' 03.1"	45.20±4.17	0.33±0.03	0.44±0.04	0.31±0.03
Y.S-9	38° 46' 15.3"	42° 36' 44.6"	10.75±0.99	0.08±0.01	0.33±0.03	0.18±0.02
Y.S-10	38° 47' 31.5"	42° 43' 30.5"	32.00±2.95	0.24±0.02	0.31±0.03	0.22±0.02
Y.S-11	38° 46' 22.4"	42° 49' 41.6"	80.85±7.45	0.60±0.06	2.30±0.21	1.34±0.12
Y.S-12	38° 47' 00.4"	42° 54' 52.7"	16.24±1.50	0.12±0.01	0.16±0.01	0.11±0.01
Y.S-13	38° 46' 01.1"	42° 59' 53.7'	41.82±3.86	0.31±0.03	0.48±0.04	0.35±0.03
Y.S-14	38° 46' 43.2"	43° 03' 41.9"	58.24±5.37	0.43±0.04	0.56±0.05	0.41±0.04
Y.S-15	38° 48' 47.6"	43° 08' 04.7"	49.29±4.54	0.33±0.03	1.35±0.12	0.73±0.07
Y.S-16	38° 52' 19.1"	43° 11' 12.9"	62.80±5.79	0.37±0.03	0.66±0.06	0.47±0.04
Y.S-17	38° 54' 24.9"	43° 10' 04.9"	56.24±5.19	0.42±0.04	0.54±0.05	0.39±0.03
Y.S-18	38° 51' 45.3"	43° 06' 14.9"	60.00±5.53	0.44±0.04	0.58±0.05	0.42±0.04
Y.S-19	38° 55' 16.7"	43° 03' 42.0"	25.53±2.35	0.12±0.01	0.49±0.04	0.26±0.01
Y.S-20	38° 56' 23.5"	43° 08' 05.3"	28.28 2.61	0.21±0.03	0.86±0.08	0.47±0.03
Y.S-21	38° 57' 08.6"	43° 14' 30.1"	18.65±1.72	0.14±0.01	0.18±0.02	0.13±0.01
Y.S-22	38° 56' 50.8"	43° 17' 39.1"	30.10±2.78	0.22±0.02	0.29±0.03	0.21±0.02
Y.S-23	38° 57' 41.5"	43° 19' 27.5"	68.45±6.31	0.51±0.05	2.07±0.19	1.49±0.14
Y.S-24	38° 58' 46.7"	43° 21' 23.8"	20.55±1.89	0.15±0.01	0.20±0.02	0.14±0.01
	Average		**40.43±3.73**	**0.29±0.03**	**0.75±0.07**	**0.47±0.04**
	Maximum		**80.85±7.45**	**0.60±0.06**	**2.30±0.21**	**1.49±0.14**
	Minimum		**10.00±0.92**	**0.08±0.01**	**0.14±0.01**	**0.08±0.01**

Table 2. The C_{Rn}, E_s, E_m and EC_{Ra} values of surface water sample in autumn period (Kayakökü and Doğru, 2019).

| Sample ID	Sample locations		C_{Rn} (Bq/m³)	E_s (Bq/m².h)×10⁻¹	E_m (Bq/m³.h)×10⁻³	EC_{Ra} (Bq/m³)
	Latitude	Longitude				
Y.S-1	38° 29' 04.3''	42° 29' 22.5''	a	a	a	a
Y.S-2	38° 30' 02.8''	42° 23' 39.8''	a	a	a	a
Y.S-3	38° 30' 03.1''	42° 18' 03.4''	48.59±4.48	0.36±0.03	1.47±0.14	0.80±0.07
Y.S-4	38° 33' 17.7''	42° 22' 11.4''	125.33±11.60	1.15±0.11	4.70±0.43	2.57±0.24
Y.S-5	38° 36' 26.5''	42° 24' 30.9''	28.76±2.65	0.45±0.04	0.66±0.06	0.55±0.05
Y.S-6	38° 39' 05.3''	42° 28' 14.7''	65.00±5.99	0.48±0.04	2.00±0.18	1.18±0.11
Y.S-7	38° 42' 56.9''	42° 26' 29.8''	86.43±7.97	0.64±0.06	2.61±0.24	1.43±0.13
Y.S-8	38° 44' 55.7''	42° 32' 03.1''	46.50±4.29	0.34±0.03	1.45±0.13	0.84±0.08
Y.S-9	38° 46' 15.3''	42° 36' 44.6''	a	a	a	a
Y.S-10	38° 47' 31.5''	42° 43' 30.5''	54.92±5.06	0.47±0.04	1.96±0.18	1.08±0.10
Y.S-11	38° 46' 22.4''	42° 49' 41.6''	171.17±15.80	1.27±0.12	5.19±0.48	3.28±0.26
Y.S-12	38° 47' 00.4''	42° 54' 52.7''	45.14±4.16	0.32±0.03	1.84±0.17	1.10±0.10
Y.S-13	38° 46' 01.1''	42° 59' 53.7'	60.55±5.53	0.45±0.04	0.89±0.08	1.06±0.10
Y.S-14	38° 46' 43.2''	43° 03' 41.9''	a	a	a	a
Y.S-15	38° 48' 47.6''	43° 08' 04.7''	a	a	a	a
Y.S-16	38° 52' 19.1''	43° 11' 12.9''	44.21±4.08	0.33±0.03	1.36±0.13	0.80±0.07
Y.S-17	38° 54' 24.9''	43° 10' 04.9''	a	a	a	a
Y.S-18	38° 51' 45.3''	43° 06' 14.9''	60.00±5.53	0.44±0.04	1.85±0.17	1.09±0.10
Y.S-19	38° 55' 16.7''	43° 03' 42.0''	72.45±6.68	0.53±0.05	2.23±0.21	1.32±0.12
Y.S-20	38° 56' 23.5''	43° 08' 05.3''	28.28±2.61	0.21±0.02	0.38±0.04	0.42±0.04
Y.S-21	38° 57' 08.6''	43° 14' 30.1''	36.80±3.39	0.27±0.02	0.50±0.05	0.58±0.05
Y.S-22	38° 56' 50.8''	43° 17' 39.1''	a	a	a	a
Y.S-23	38° 57' 41.5''	43° 19' 27.5''	a	a	a	a
Y.S-24	38° 58' 46.7''	43° 21' 23.8''	a	a	a	a
Average			**64.94±5.99**	**0.51±0.05**	**1.94±0.18**	**1.21±0.11**
Maximum			**171.17±15.80**	**1.27±0.12**	**5.19±0.48**	**3.28±0.26**
Minimum			**28.28±2.61**	**0.21±0.02**	**0.38±0.04**	**0.42±0.04**

[a] Water samples could not be taken
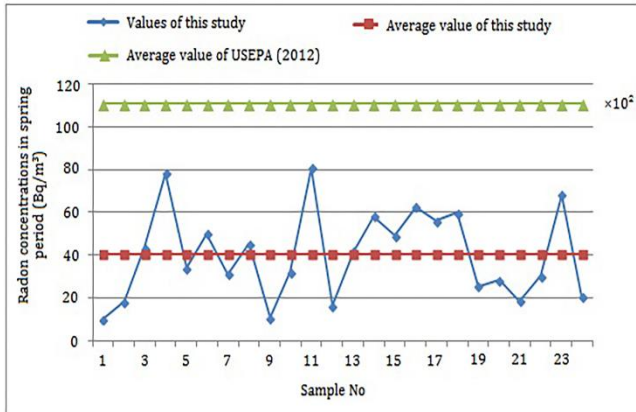
Figure 4. Comparison of radon concentration values in surface water samples of spring period with the value recommended by United States Environmental Protection Agency (USEPA, 2012).

Figure 5. Comparison of radon concentration values in surface water samples of autumn period with the value recommended by United States Environmental Protection Agency (USEPA, 2012).

The highest C_{Rn}, E_s, E_m values in spring water samples were found in the sample Y.S-11. Similarly, the highest C_{Rn}, E_s, E_m and EC_{Ra} values in autumn water samples were found in the sample Y.S-11. While the lowest C_{Rn} value obtained for water samples belonged to the spring period Y.S-1 sample with 10.00 ± 0.92 Bq/m³, the highest C_{Rn} value belonged to the autumn period Y.S-11 sample with 171.17 ± 15.80 Bq/m³. While the lowest E_s value belonged to the spring period YS-9 sample with $(0.08\pm0.01)\times10^{-1}$ Bq/m².h, the highest E_s value belonged to the autumn period YS-11 sample with $(1.27\pm0.12)\times10^{-1}$ Bq/m².h. E_m value was calculated as the lowest with $(0.14\pm0.01)\times10^{-3}$ Bq/m³ at Y.S-1 sample in spring period and the highest with $(5.19\pm0.48)\times10^{-3}$ Bq/m³ at Y.S-11 sample in autumn period.
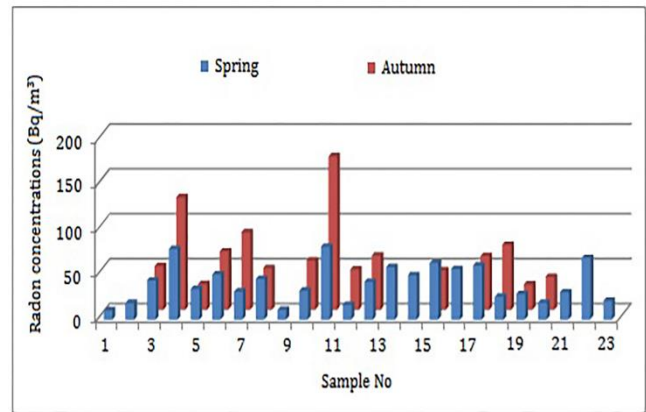

Figure 6. Seasonal variation of radon concentration in samples

Finally, in all water samples, EC_{Ra} value was determined to be the lowest with $(0.08\pm0.01)\times10^{-1}$ Bq/m³ at Y.S-23 sample in spring period and the highest with $(3.28\pm0.26)\times10^{-1}$ Bq/m³ at Y.S-9 sample in autumn period.

Comparison of radon concentration averages obtained for surface water samples in this study with the results obtained in similar studies was given in Table 3.
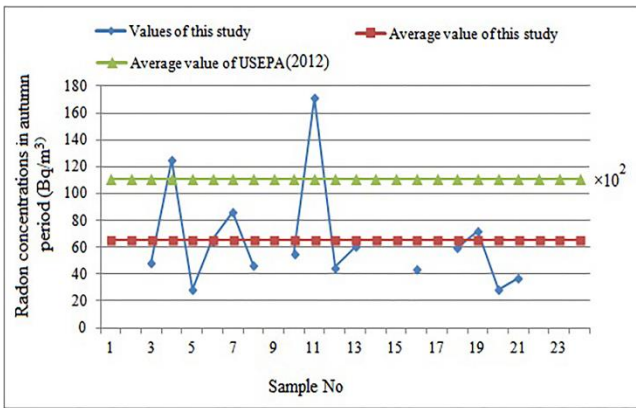
Table 3. Comparison of radon concentration averages obtained for water samples in this study with the results obtained in similar studies

Countries	Concentration of ^{222}Rn (Bq/m^3)	Reference
England (English Lake District)	53.7±8.15-1130.74±35.92	Al-Masri and Blackburn, 1999
Turkey (Yeşilırmak River)	280±40-1080±300	Oner et al., 2009
Egypt (Manzala Lake)	(1.720 – 6.400) ×10^3	Yousef et al., 2017
China (Yunlong Lake) (average)	2.154 ×10^3	Yang et al., 2020
India (Varahi River)	(2.07±0.84) ×10^3	Somashekar and Ravikumar, 2010
India (Markandeya River) (average)	(9.30±1.45) ×10^3	Somashekar and Ravikumar, 2010
UNSCEAR	10×10^3	UNSCEAR, 2000
USEPA	11.1×10^3	USEPA, 2012
EPA	11×10^3	EPA, 2000
WHO	100×10^3	WHO, 2008
Turkey (Van Lake) (average)	40.43±3.73 (spring) 64.94±5.99 (autumn)	Present Study

Baykara and Doğru (2006) collected 14 water samples from the region of the North and East Anatolian Active Faults. By using the passive radon measurement method, they calculated the highest radon concentration, effective radium content and radon diffusion rate in water samples as 3319.3 Bq/m^3, 270.5 Bq/m^3 and 0.470 Bq/m^2.h, respectively (Baykara and Doğru, 2006).

Bal and Doğru (2013), passively examined radon concentrations in the water samples they received from the radon monitoring stations they established in the Sivrice Fault Zone. As a result of the study, it was seen that the radon concentration values of the water samples taken in autumn and spring varied between 2750±736 Bq/m^3 and 4624±1251 Bq/m^3 with 4464±1524 Bq/m^3 and 7163±1941 Bq/m^3, respectively (Bal and Doğru, 2013).

According to the study conducted by Zorer et al., (2013), the radon concentration in lake water around Van Lake varied between 47.80 Bq/m^3 and 354.86 Bq/m^3 (Zorer et al., 2013).

United States Environmental Protection Agency (USEPA) recommends the maximum value of the radon activity level as 11.1 Bq/L (11.1×10^3 Bq/m^3) in drinking water (USEPA, 2012). The United Nations Scientific Committee on the Effects of Atomic Radiations (UNSCEAR) has suggested the radon concentration in drinking water must lies between 4 and 40 Bq/L (UNSCEAR, 2008).

In present study, the radon concentration values calculated in all samples were lower than 100 Bq/L (100×10^3 Bq/m^3) recommended for drinking water by European Commission (EU, 2001) and World Health Organization (WHO, 2004).

The results obtained in water samples of this study were found to be lower than the results obtained in the above studies and the limit values given for water.

Considering Table 1, Table 2 and Figure 6, when the C_{Rn}, E_s, E_m and EC_{Ra} values obtained for the surface water samples taken in spring and autumn were compared seasonally, it was observed that the C_{Rn}, E_s, E_m and EC_{Ra} values in spring were lower than those from autumn. This may result from the high rainfall in spring and excessive flows from other water sources into the lake.

4. Conclusions

In this study, the seasonal variation in the C_{Rn}, E_s, E_m and EC_{Ra} values in the surface water samples taken in spring and autumn from 24 different points of Van Lake was investigated. Measurements were made using the Passive Radon Detector System (RadoSYS system).

At the end of the study, the highest C_{Rn}, E_s, E_m and EC_{Ra} values were calculated for the S-11 point. The Suphan fault line passes through the region where S-11 is located, and this area densely contains volcanic sediments and late Miocene-Quaternary. In a study, Ramola et al. (2006) discovered that the radon level was higher in the areas comprised of granite, quartz-porphyry, schist and phyllite slates, and lower in the areas with sedimentary rocks.

The radon measurement results obtained in this study were found to be lower than the limit values permitted by USEPA (2012), UNSCEAR (2008), EU (2001) and WHO (2004) and results obtained in similar studies.

When the results obtained for the C_{Rn}, E_s, E_m and EC_{Ra} parameters were compared seasonally, it was seen that the results obtained in the autumn period were higher than those in the spring period.

References

Alali, A.E., Al-Shboul, K.F., Yaseen, Q.B., and Alaroud, A., 2019. Assessment of radon concentrations and exposure doses in dwellings surrounding a high capacity gas turbine power station using passive measurements and dispersion modeling. Journal of Environmental Radioactivity, 196, 9–14.

Alkan, H., and Göksel, S.A., 1975. Türkiye Kaplıca ve Maden Sularının Doğal Radyoaktiviteleri, Sularda Radon Tayini, T. B. T. A. K. 5. Bilim Kongresi, Ankara, 229-241.

Yaramış, B., 1985. Nükleer Fizik. 1, İ.T.Ü. Fen-Edebiyat Fakültesi, İstanbul.

Al-Masri, M.S., and Blackburn, R., 1999. Radon-222 and related activities in surface waters of the English Lake District. Applied Radiation and Isotopes, 50, 1137-1143.

Bal, S.Ş., and Doğru, M., 2013. Su ve toprak örneklerinde radon gazı yayılımının mevsimsel değişiminin incelenmesi. BEÜ Fen Bilimleri Dergisi, 2(2), 192-196.

Baykara, O., and Doğru, M., 2006. Measurements of radon and uranium concentration in water and soil samples from East Anatolian Active Fault Systems (Turkey), Radiat. Meas., 41, 362–367.

Bohus-Saja, L., Gomez, J., Capote, T., Greaves, E.D., Herrera, O., Salazar, V., and Smith, A.J., 1997. Environ. Radioact., 35, 305-312.

Büyükuslu, H., Özdemir, F.B., Öge, T.Ö., and Gökce, H., 2018. Indoor and tap water radon (^{222}Rn) concentration measurements at Giresun University campus areas. Applied Radiation and Isotopes, 141, 95–100.

EPA (Environmental Protection Agency), 2000. Final Rule for Non-Radon Radionuclides in Tap Water, Technical Fact Sheet, EPA, 815-F-00-013, 2000.

EU (European Commission), 2001. Commission recommendation of 20th December 2001 on the protection of the public against exposure to radon in drinking water suplies (2001/928/Euratom). Off. J. Eur. Comm. L:344/85.

Ilani, S., Minster, T., Kronfeld, J., and Even, O., 2006. The source of anomalous radioactivity in the springs bordering the Sea of Galilee, Israel. Journal of Environmental Radioactivity, 85, 137-146.

Jönsson, G., Baixeras, C., Devantier, R., Enge, W., Font, L.L., Freyer, K., Ghose, R., and Treutler, H.C., 1999. Soil radon levels measurements with SSNTD's and the soil radium content, Radiat. Meas., 31, 291-294.

Kayakökü, H., Karatepe, Ş., and Doğru, M., 2016. Measurements of radioactivity and dose assessments in some building materials in Bitlis, Turkey Applied Radiation and Isotopes, 115, 172-179.

Kayakökü, H., and Doğru, M., 2019. "Seasonal Radon Measurements in Surface Water Samples from Van Lake, Turkey" XII. International Conference on Nuclear Structure Properties (NSP 2019), Poster Presentation, 11-13 September 2019, Bitlis, Turkey.

Oner, F., Yalim, H.A., Akkurt, A., and Orbay, M., 2009. The measurements of radon concentrations in drinking water and the Yeşilırmak River water in the area of Amasya in Turkey Protection Dosimetry, 133(4), 223–226.

Ramola, R.C., Choubey, V.M., Prasad, Y., Prasad, G., and Bartarya, S.K., 2006. Variation in radon concentration and terrestrial gamma radiation dose rates in relation to the lithology in southern part of Kumaon Himalaya, India. Radiat. Meas., 41: 714-720.

Sannappa, J., Chandrashekara, M.S., and Paramesh, L., 2006. Spatial distribution of radon and thoron concentrations indoors and their concentrations in different rooms of buildings. Indoor and Built Environment, 15(3), 283-288.

Shashikumar, T.S., Chandrashekara, M.S., Nagaiah, N., and Paramesh, L., 2009. Variations of radon and thoron concentrations in different types of dwellings in Mysore city, India. Radiation Protection Dosimetry, 133(1), 44-49.

Somashekar, R.K., and Ravikumar, P., 2010. Radon concentration in groundwater of Varahi and Markandeya river basins, Karnataka State, India. J Radioanal Nucl Chem., 285, 343–351.

Tokonami, S., Takahashi, H., Kobayashi, Y., Zhuo, W., and Hulber, E., 2005. Up-to-date radon-thoron discriminative detector for a large scale survey, Rev. Sci. Instrum. 76, 113-505.

Turhan, Ş., Demir, K., and Karataşlı, M., 2018. Radiological evaluation of the use of clay brick and pumice brick as a structural building material. Applied Radiation and Isotopes, 141, 95–100.

UNSCEAR (United Nations Scientific Committee on the Effects of Atomic Radiations), 2000. Sources and effects of ionizing radiation. Report to the General Assembly with scientific annexes (pp. 97-105). United Nations, New York, Annexure B.

UNSCEAR (United Nations Scientific Committee on the Effects of Atomic Radiations), 2008. Report to General Assembly with Scientific annexes. United Nations Sales Publications. United Nations, New York.

USEPA (United States Environmental Protection Agency), 2012. Edition of the Drinking Water Standards and Health Advisories. EPA 822-S-12-001 Office of Water U.S., Environmental Protection Agency, Washington, DC.

WHO (World Health Organization), 2004. Guidelines for Drinking-Water Quality. Vol. 1. Recommendations, third ed., Geneva.

WHO (World Health Organization), 2008. Guidelines for Drinking-Water Quality. Vol. 1. Recommendations, third ed., Incorporating the First and Second Addenda, Geneva.

Varol, S., 2011. Gross alpha and beta radioactivity in groundwaters. Journal of Engineering Science and Design, 1(3), 101-106.

Yang, J., Yu, Z., Yi, P., Frape, K.S., Gong, M., and Zhang, Y., 2020. Evaluation of surface water and groundwater interactions in the upstream of Kui River and Yunlong Lake, Xuzhou, China. Journal of Hydrology, 583, 124549.

Yaramış, B., 1985. Nükleer Fizik. 1, İ.T.Ü. Fen-Edebiyat Fakültesi, İstanbul.

Yousef, H.A., El- Farrash, A.H., and Magdy, A., 2017. Radon Levels in Surface Water Samples from Manzala Lake East Nile Delta, Egypt using Nuclear Track Detectors. Journal of Nuclear and Particle Physics, 7(2), 36-42.

Zorer, Ö.S., Şahan, T., Ceylan , H., Doğru, M., and Şahin, S., 2013. ^{238}U and ^{222}Rn activity concentrations and total radioactivity levels in lake waters, J. Radioanal. Nucl. Chem., 295, 1837–1843.